P–T paths reconstruction of a collisional event: The example of the Thiviers-Payzac Unit in the Variscan French Massif Central

Manuel Duguet, Nicole Le Breton, Michel Faure

P–T paths reconstruction of a collisional event: The example of the Thiviers-Payzac Unit in the Variscan French Massif Central

Manuel Duguet [a], Nicole Le Breton [a], and Michel Faure[a]
[a]Institut des Sciences de la Terre d'Orléans (ISTO), UMR6113 CNRS/Université d'Orléans, Bâtiment Géosciences, Rue de Saint Amand, BP 6759, F-45067 Orléans Cedex 2, France
Received 2 May 2006; accepted 1 April 2007. Available online 19 April 2007.

Abstract

Because of late metamorphic and tectonic overprints, the reconstruction of prograde parts of *P–T* paths is often difficult. In the SW Variscan French Massif Central, the Thiviers-Payzac Unit (TPU) is the uppermost allochthon emplaced above underlying units. The TPU experienced a Barrovian metamorphism coeval with a top-to-the-NW ductile shearing (D2 event) in Early Carboniferous times (*ca.* 360–350 Ma). The tectonic setting of the D2 event, compression or synconvergence extension, remains unclear. Using the THERMOCALC software and the model system MnNCKFMASH, the peak *P–T* conditions are estimated from garnet rims and matrix minerals and the prograde evolution is deduced from garnet core compositions. The combination of these two approaches demonstrates that the TPU experienced pressure and temperature increases before reaching peak conditions at 6.6–9.0 +/− 1.2 kbar and 615–655 +/− 35 °C. This kind of *P–T* path shows that the regional D2 event corresponds to crustal thickening.

Keywords: *P–T* path reconstruction; Barrovian metamorphism; Pseudosections; Variscan orogeny; French Massif Central

Abbreviations: alm, almandine; an, anorthite; ap, apatite; bi, biotite; cel, celadonite; chl, chlorite; cd, cordierite; east, eastonite; g, garnet; gr, graphite; grs, grossular; ksp, K-feldspar; ky, kyanite; ilm, ilmenite; mo, monazite; mu, muscovite; pa, paragonite; pl, plagioclase; pyr, pyrope; q, quartz; rt, rutile; liq, silicate melt; sill, sillimanite; spe, spessartite; st, staurolite; fst, Fe-staurolite; mst, Mg-staurolite; xe, xenotime

1. Introduction

A main characteristic of orogens is a polyphase deformation history involving various tectonic processes such as burial of crustal slices followed by exhumation of deep metamorphic rocks by nappe stacking, syn-orogenic to post-orogenic extension and tectonic denudation. The late orogenic processes alter, or even erase, at least part of the early structural, textural and mineralogical features of the metamorphic evolution. Thus, relicts of prograde parageneses and kinematic criteria typical of crustal thickening are often very tenuous. The reconstruction of the prograde part of a *P–T* path coeval with a compression stage is therefore difficult. However, this problem can be overcome when the metamorphic series contain garnet-bearing metapelitic rocks which have undergone metamorphism with a peak at the amphibolite facies conditions. Indeed, during the prograde history, while most of the minerals in metapelites reach equilibrium at medium temperature because reaction and diffusion rates become high enough to allow the homogenization of phases, garnet tends to preserve its chemical growth zoning. This point is not very relevant for conventional

thermobarometry because the minerals which were in equilibrium with the core of the garnet at a given stage of the prograde history have disappeared, or have changed in composition, in response to a *P–T* increase. Even inclusions trapped in garnet are probably no longer in equilibrium with their host mineral because of late exchange processes. On the other hand, as outlined by several authors (*e.g.* [Vance and Mahar, 1998] and [Stowell and Tinkham, 2003]), the chemical growth zoning preserved in garnet enables the use of *P–T* pseudosections contoured for garnet composition with different isopleths in order to estimate *P–T* conditions corresponding to garnet nucleation. Each *P–T* pseudosection, calculated with the thermodynamic software THERMOCALC (Powell and Holland, 1988) coupled with its internally consistent thermodynamic database (Holland and Powell, 1998), is valid for a unique chemical composition in a model system. If it can be assumed that the analysed bulk rock composition was the effective chemical composition of the equilibrated system at the time of crystallization of garnet cores, the *P–T* pseudosection drawn for this composition and showing different isopleths for garnet can then be used as a thermobarometric tool allowing the determination of one "point" on the prograde part of the *P–T* path followed by the garnet–bearing metapelites. The second point of the *P–T* path, *i.e*. the peak *P–T* conditions, cannot be determined easily with a pseudosection because the effective chemical composition of the equilibrated system at this highest metamorphic temperature has to be estimated by removing from the whole system those parts of zoned garnet porphyroblasts which were out of equilibrium at that time. Fortunately, when all the phases, except garnet, are homogeneous in the rock, the highest *P–T* conditions can be estimated by using the multi-equilibrium approach of thermobarometry with the mode "average *P–T*" of the software THERMOCALC ([Powell and Holland, 1994] and [Worley and Powell, 2000]). Therefore, in short, combining a pseudosection and the results of multi-equilibrium thermobarometry should provide details of at least a part of the prograde *P–T* path followed by garnet metapelites last transformed at the amphibolite facies conditions.

This combined thermobarometric approach is used in the Variscan French Massif Central in order to document the *P–T* evolution of the uppermost tectonic unit, called the Thiviers-Payzac Unit (TPU), emplaced by top-to-the NW ductile shearing above the Upper Gneiss Unit (UGU). The TPU has been chosen as a target for the investigation of the *P–T* path related to top-to-the NW shearing since this crustal slice is little affected by other tectonic events ([Faure et al., 1997] and [Roig and Faure, 2000]). In the tectono–metamorphic evolution of the French Massif Central, this top-to-the NW event corresponds to a second tectonic event (D2). In the southern part of the Variscan Belt, the first event (D1) took place during the Early Devonian and corresponds to a top-to-the SW nappe emplacement. This D1 event is related to the collision between Gondwana to the south and Armorica to the north (*e.g.* [Matte, 1991], [Faure et al., 2004] and [Faure et al., 2005]). The top-to-the NW event (D2) occurred in Late Devonian – Early Carboniferous times and reworks the stack of nappes previously formed by the D1 event. The D2 event is not younger than 350 Ma since the contact between the TPU and its footwall is locally reworked by a sinistral wrench fault coeval with pluton emplacement dated by $^{40}Ar/^{39}Ar$ method on biotite at 346 +/− 3.5 Ma (Roig et al., 1996). The D2 event has a regional extent since it affects the whole French Massif Central and also the southern part of the Massif Armoricain. However, the geodynamics and tectonic setting of the D2 event are still matter of debate. Indeed, several contradictory models have been proposed to explain the top-to-the NW shearing. The D2 event has been related either to transpressional tectonics during a single orogenic cycle (Brun and Burg, 1982), or to nappe thrusting (Bouchez and Jover, 1986), or to syn-orogenic extension (Mattauer et al., 1988), or to a second compressional cycle after a short period of rifting during Upper Devonian ([Faure et al., 1997] and [Faure et al., 2005]). Thus, to

reconstruct *P–T* paths experienced by different units is a crucial point to decipher the tectonic setting of the D2 event or, in other words, to know whether the D2 event took place during an extensional tectonic setting or during a compressional one. Indeed, none of the previously exposed models takes into account thermobarometric data. The scarcity of available thermobarometric data concerning the D2 event precludes any interpretation to be correctly assessed. It is also worth underlining that a great part of the tectonic units formed during D1 and D2 events are widely reworked during the Late Carboniferous by syn- and post-orogenic extensional tectonics coeval with the emplacement of numerous granitic plutons (Faure, 1995). Thus, such first hand quantitative information together with a detailed analysis of the thermobarometric results will enable to discuss the tectonic evolution of this part of the Variscan Belt.

2. Geological setting

2.1. Structural framework of the French Massif Central

The Variscan French Massif Central consists of a stack of nappes formed by polyphase tectonics (*e.g.* [Matte, 1991], [Ledru et al., 1989], [Faure et al., 1997] and [Faure et al., 2005]). From south to north, and from bottom to top, the following units are recognized (Fig. 1): i) a Visean-Early Namurian Foreland Basin; ii) a Palaeozoic Fold and Thrust Belt; iii) a low to medium grade metamorphic domain generally subdivided into the Para-autochthonous Unit (PAU) and the Lower Gneiss Unit (LGU) (omitted on Fig. 1a for clarity but shown on Fig. 1b); iv) the Upper Gneiss Unit (UGU) which includes eclogitic relics. These high pressure rocks were formed during continental subduction of Gondwana below Armorica, although true ophiolites are lacking in the Massif Central; and v) an uppermost allochthonous crustal slice called the Thiviers-Payzac Unit (TPU). The TPU, which crops out in the southwest part of the Massif Central (Fig. 1a), has received different local names depending on the area, namely the “Gartempe Unit” in North Limousin, the “Thiviers-Payzac Unit *stricto sensu*” in South Limousin, the “Leyme Unit” in Quercy, the “Saint-Sernin-sur-Rance Nappe” in Rouergue. Nevertheless, similar lithological, metamorphic and structural features are recognized in all these areas ([Guillot, 1981], [Floc'h, 1983], [Santallier and Floc'h, 1989] and [Roig et al., 1996]). The TPU consists of metagreywackes, metasandstones and metapelites with minor amounts of quartzites, graphite schists, marbles and amphibolites. The foliation presents a well-developed NW–SE trending mineral and stretching lineation along which shear criteria such as sigmoidal mica, quartz and biotite pressure shadows, or sigma-type porphyroblasts of garnet and staurolite indicate a top-to-the NW shearing. The thermobarometric study reported hereafter is limited to the TPU which outcrops in the Quercy area, that is to the “Leyme Unit” shown in Fig. 1.

2.2. Large scale structure of the TPU in the Quercy area

In the Quercy area, several allochthonous sheets are distinguished from top to bottom, (Guillot et al., 1992; Fig. 1b). The uppermost unit, the TPU, consists of metagreywackes and metapelites metamorphosed under medium pressure/medium temperature conditions (Guillot et al., 1992). Metapelites (paragneisses and micaschists) are intruded by two types of plutonic rocks: an Ordovician porphyritic granite which has been extensively foliated and transformed into augen–gneiss, and Devonian dioritic plutons. Similar diorites have been dated elsewhere in the French Massif Central between 375 and 360 Ma (Pin and Paquette, 2002). The margins of the diorite plutons are deformed and the resulting foliation is concordant with the regional one. The TPU is a NW–SE trending kilometre-scale synform (Fig. 2). The folded surface is

not only a bedding surface but also a previous foliation developed during a subhorizontal synmetamorphic shearing.

The TPU tectonically overlies ortho- and paragneisses locally called the “Saint-Paul-de-Vern Unit” (Guillot et al., 1989). Our own field survey suggests that this “Saint-Paul-de-Vern Unit” is composite and comprises in fact two parts belonging, from top to bottom, to the UGU and to the LGU, respectively. Biotite–sillimanite migmatitic gneiss, similar to those described in the UGU elsewhere in the French Massif Central, are separated from the LGU by a mylonitic contact. In the present state of knowledge, no eclogitic relic has been found in the UGU of the Quercy area in which widespread garnet, kyanite and sillimanite indicate Barrovian metamorphic conditions.

Lastly, to the east, the LGU is separated from the underlying PAU by the Argentat ductile normal fault. Along the Argentat fault, NW–SE trending slickenlines indicate that the western hangingwall moved to the NW. The Argentat fault is a polyphase tectonic contact since an early thrust contact is reworked during the Middle to Late Carboniferous by an extensional tectonic event which began around 330 Ma in the North Massif Central ([Faure, 1995] and [Roig et al., 2002]). The PAU consists of micaschists that have been metamorphosed under Barrovian conditions estimated around 4–5 kbar and 600 °C (Feix, 1988). In the vicinity of the Argentat fault, the Barrovian assemblages (garnet + biotite +/− staurolite) were retrogressed during the extensional tectonics. At the same time, leucogranitic plutons intruded the micaschists of the PAU and induced the crystallization of biotite and andalusite in the thermal aureole.

2.3. Structural pattern and kinematics of the TPU in the Quercy area

A detailed structural analysis of the Quercy area is beyond the scope of this paper since its main object is to establish thermobarometric constraints for the TPU. As stated above, the NW–SE trending foliation is involved in kilometre-scale NE vergent or upright folds, but, as everywhere in the French Massif Central, it developed with a flat-lying attitude (e. g. [Guillot, 1981], [Floc'h, 1983], [Bouchez and Jover, 1986], [Feix, 1988], [Ledru et al., 1989], [Santallier and Floc'h, 1989], [Matte, 1991], [Roig and Faure, 2000] and [Faure et al., 2005]). The foliation bears a NW–SE trending stretching and mineral lineation parallel to the axes of intrafolial folds. Crenulation lineation parallel to the mineral lineation develops locally (Fig. 2). These planar and linear microstructures are coeval with the metamorphic minerals: biotite, muscovite, garnet, and staurolite. At the outcrop scale, macroscopic shear criteria are rare due to the pelitic nature of the rocks. However, in thin sections cut parallel to the NW–SE lineation and perpendicular to the foliation, numerous kinematic indicators such as asymmetric quartz and biotite pressure shadows around garnet porphyroblasts, sigmoidal inclusion trails in staurolite and garnet poikiloblasts, biotite and muscovite micafishes and shear bands show a top-to-the NW shearing (Fig. 3). When the foliation is vertical, shear criteria give a consistent dextral sense of shear. Since kinematics do not change on both flanks of NE-vergent recumbent folds, it is likely that shearing was coeval with this kilometre-scale folding and the emplacement of the TPU above higher grade metamorphic units.

3. Petrography and mineral chemistry

3.1. Parageneses and chemical compositions of metapelites

To constrain the *P–T* conditions of prograde metamorphism of the TPU in the Quercy area, six garnet–biotite–muscovite micaschists were sampled (locations are shown in Fig. 2 and mineral assemblages are given in Table 1.). All these metapelites display a well-developed schistosity defined by the preferred orientation of muscovite and biotite. Biotite is not only present as small flakes underlying the planar structure but also as lozenge-shaped crystals which represent early porphyroblasts. The asymmetry of these "mica-fishes" is useful to determine sense of shear. A last generation of biotite appears as undeformed crystals with their clivage perpendicular to the schistosity and can be interpreted as postkinematic. Quartz and plagioclase form a fine granoblastic aggregate between the mica flakes. Garnets commonly occur as euhedral or subhedral blasts. They range in size between 0.4 and 3.0 mm. The cores are frequently very poikilitic and contain small inclusions of quartz, plagioclase, Fe–Ti oxide, monazite, xenotime, apatite in all samples, and graphite in sample F4. The rims are poorer in inclusions. In some grains, inclusion trails define an internal foliation (Si) which is, in sample F6, connected to the external foliation (Se). These sigmoidal inclusions indicate that garnet grew during the top-to-the NW deformation event (Fig. 3d). One of these garnet-bearing metapelites (F24) contains also staurolite. There are two textural populations of staurolite. The first one is elongated in the foliation or shows sigmoidal patterns that indicate a synkinematic crystallization (Fig. 3c). The second one is oriented across the foliation and is therefore postkinematic. Both populations are rich in quartz and Ti–Fe oxides inclusions. No sillimanite or kyanite is observed in any of the six metapelites.

The chemical bulk compositions of these six metapelites are given in Table 2. Sample F13 is the only sample significantly poorer in aluminium, magnesium and alkali and richer in silicium than the other samples, but it contains the same phases as more aluminuous rocks such as F4, F6, F7 or F29. The staurolite-bearing metapelite F24 has just slightly higher aluminium and iron contents than samples F4, F6, F7 and F29.

[a] $(Al_2O_3–3K_2O–CaO–Na_2O)/(Al_2O_3–3K_2O–CaO–Na_2O + FeO + MgO)$.

3.2. Mineral chemistry

Element analyses of minerals were performed on the CAMECA CAMEBAX electron microprobe jointly managed by BRGM, CNRS and the University of Orléans. For point analyses, the accelerating voltage was 15 kV and the beam current was 10 nA. Counting time was 10 s on peak and 10 s on background for all elements. Natural and synthetic silicates and oxides were used as standards. The collected data were corrected with the ZAF procedure by use of the PAP software provided by CAMECA. For X-ray maps, the beam current was 50 nA.

3.2.1. Garnet

3.2.1.1. Garnet zoning

Garnet chemistry is first investigated using electron microprobe point analyses. The structural formulae given in Table 3 are normalized to eight cations. Then, an empirical ferric iron

estimate is made by bringing the sum of the positive charges to twenty-four when it is initially lower than this value. In the investigated garnets, the amount of ferric iron is negligible (Table 3), which is a good basis to undertake a thermobarometic study.

Compositional profiles across garnet (Fig. 4) and X-ray composition maps (Fig. 5) show for all samples an obvious chemical zoning. In general, both the almandine and pyrope contents increase from core to rim whereas the spessartite content shows a more or less pronounced "bell shaped profile", with a Mn-rich core and Mn-poor rims. Considering now the grossular component, two types of garnets must be distinguished: those with a flat profile (samples F6, F13 and F24) and those with Ca-rich cores characterized by a high density of inclusions and Ca-poor rims nearly devoid of inclusions (samples F4, F7 and F29).

Between samples, compositional profiles differ not only in shape but also in amplitude (Fig. 4). For example, in the garnet cores, almandine mole fractions are in the range 0.40–0.72 while the grossular contents show a large variation from 0.05 to 0.30. Garnet rims exhibit also composition differences between grains but to a lesser extent than the cores.

Some zoning features appears only on Ca and Y distribution maps. In sample F13, garnet has a Ca-poor annulus around a large euhedral core richer in grossular and truncated at one point (arrow in Fig. 5). Bands of high-Y content correspond exactly to the outer shell of the euhedral Ca-richer core. Moreover, in this sample, the high-Y zones are in close association with inclusions of monazite (Fig. 6). In garnet from F7, the Ca zoning is pronounced, with a steep compositional gradient between a Ca-rich core (X_{Ca}^{g} about 0.28) and Ca-poor rims (X_{Ca}^{g} about 0.08). The outlines of the concentric zones are anhedral (arrow in Fig. 5 for example). Moreover, an Y-rich annulus corresponds to the Ca-poor outermost portion of the garnet, with a rather diffuse outer limit and a rather sharp inner border.

A final observation must be pointed out: whatever the garnet is (in samples F6, F7, F13, and F24 on Fig. 5), Y, like Mn, is not enriched at the utmost edge of the grains.

3.2.1.2. Interpretation of garnet zoning

The "bell shaped profile" for spessartite (F4, F7) was first interpreted by Hollister (1966) as the result of the Mn fractionation during prograde garnet growth. The increase in almandine content and, to a lesser extent, in pyrope content towards the rims corresponds to the spessartite decrease as garnet progressively crystallizes. These profile shapes are typical for garnets grown at amphibolite facies conditions (Spear et al., 1990). The reason why some zoning features appear only on Ca and Y maps was given by Pyle and Spear (1999) who emphasized that the diffusivity of Y in garnet is much slower than the diffusivities of Mg, Fe and Mn. So Y is able to record some early prograde events which cannot be observed in distribution maps of Mg, Fe and Mn because diffusive re-equilibration occurred as temperature was increasing. Ca would behave like Y and one can expect therefore to extract much more information about the prograde evolution of the garnet metapelites from Ca and Y distribution maps than from the other composition maps.

Some examples show that the composition variability of garnet cores and rims is not only due to various bulk compositions of the host rocks. Samples F4 and F29, which contain respectively 1.99 and 0.47 wt. % CaO (Table 2), both have garnet cores with about 23 mol% grossular (Table 3) while the sample F6, with the same mineral assemblage as F4 and a bulk CaO content of 0.89 wt. % (Table 2), contains garnets with only 5 mol% grossular (Table 3).

Therefore, the differences between garnet compositions of the investigated samples must be explained, at least partly, with the help of a thermobarometric study.

Some compositional characters of the garnet crystals provide constraints for application of thermobarometry. Garnets of sample F6 and F24 show a continuous and limited growth zoning which is unaffected by either retrograde breakdown of garnet (since no enrichment in Mn and Y right at the crystals rims is observed), or by late local exchange with ferromagnesian minerals (since the Fe and Mg distributions are not disturbed in the outermost part of the grains). In contrast, garnet in F7 shows a discontinuous zoning, especially for Ca and Y. Its Y-rich annulus and its anhedral Ca-rich core indicate that it has suffered dissolution prior to an overgrowth, following Pyle and Spear (1999) who proposed that the high-Y annuli observed in garnet of staurolite-zone metapelites "*may form by garnet overgrowth of proximal matrix enriched in Y due to garnet consumption during discontinuous staurolite-forming reactions*". In this process, the accessory minerals enriched in Y play an important role. Sample F7 does not contain any staurolite but the discussion in Section 4.4 will show that the reaction process described by Pyle and Spear (1999) and Yang and Rivers (2002) is likely to have occurred during the prograde history of the rock. Interpretation of garnet in F13 is more complex because while Y-rich bands do exist, associated with monazite inclusions (Fig. 6), they coincide with the outer shell of the euhedral Ca-rich core. This texture does not indicate a dissolution episode of the garnet. It seems therefore that only growth stages occurred during the prograde evolution of sample F13. A truncature does exist at one point (arrow on Fig. 5) but it could be due to lack of growth in contact with another mineral and not to resorption. In this case, the necessity of calculating a *P–T* pseudosection to get a better understanding of the prograde history is obvious. Lastly, as for garnets in F6 and F24, the lack of Mn and Y enrichment at the utmost edge of the grains and the lack of local disruptions of the Fe and Mg zonings in the outer shell of the garnet indicate that both net-transfer and exchange reactions affecting the garnet were negligible after its growth in samples F7 and F13. For all the garnet-bearing metapelites, it is therefore reasonable to consider garnet zoning as essentially due to a continuous or discontinuous disequilibrium growth during the prograde history in the amphibolite facies.

3.2.2. Other minerals

3.2.2.1. Biotite

Structural formulae of biotite (Table 4) are calculated on a basis of 11 oxygens without ferric iron. In a given sample, there is no chemical difference between the different biotite generations and each grain is chemically homogeneous. Both synkinematic and postkinematic biotites have generally iron mole fractions (X_{Fe}^{Bt}) between 0.48 and 0.60. Just sample F13 has biotites with a highest X_{Fe}^{Bt} around 0.65–0.70, which is in agreement with the highest value of X_{Fe}^{rock}. Ti varies from 0.07 to 0.12.

3.2.2.2. Muscovite

Structural formulae of white micas (Table 5) are calculated on a basis of 11 oxygens without ferric iron. It is assumed that the mole fraction Fe/(Fe + Mg) is the same in M1 and M2 sites. The celadonite component is not abundant in these white micas which are essentially a binary solid solution of muscovite (more than 72 mol%) and paragonite (less than 22 mol%). Muscovite is unzoned with regard to the paragonite and celadonite contents.

3.2.2.3. Plagioclase

Matrix plagioclase has anorthite contents ranging between 17 and 26 mol% (Table 6). Unfortunately, plagioclase inclusions in garnet are often too small to be analysed, except for sample F6 where they are anorthite-richer (X_{an} = 0.23) than matrix plagioclase (X_{an} = 0.18). Only in sample F13, a decrease in X_{an} from core (0.20) to rim (0.17) is obvious in matrix plagioclase.

3.2.2.4. Staurolite

Staurolite is chemically homogeneous with X_{Fe}^{St} around 0.82 (Table 7). The ZnO content is lower than 0.4 wt. %, which corresponds to X_{Zn}^{St} lower than 0.02.

4. Thermobarometry of garnet bearing metapelites

4.1. Methodology

As mentioned above, an aim of this study is to reconstruct a part of the prograde *P–T* path followed by garnet-bearing metapelites belonging to the TPU in the Quercy area in order to understand the geodynamic evolution of this crustal slice. *P–T* pseudosections calculated using THERMOCALC, the software developed by (Powell and Holland, 1988) and (Powell and Holland, 1994), are useful to characterize the early petrogenetic events which took place as garnet began to grow if it can be assumed that, at that time, matrix minerals were not zoned and that the whole rock was therefore in equilibrium. This assumption seems reasonable if garnet nucleation took place at amphibolite facies conditions. Moreover, since the investigated metapelites do not show migmatitic features, they have not lost any melt. Therefore, the analysed bulk chemical compositions (Table 2) are likely those of the reacting systems as garnet began to crystallize and, consequently, they may be used to calculate the *P–T* pseudosections. It is not possible to exclude a silica loss during subsequent metamorphism but, since all samples contain quartz, a decrease in silica content of the system would not have modified the nature of the parageneses. The model chemical system used in this study is the MnCNKFMASH system saturated with a pure H_2O fluid phase, this last point being discussed later (in Section 4.5). The activity-composition relationships are those used by Tinkham et al. (2001). It remains however that the thermodynamic data and the activity models for Mn-bearing systems are not yet perfect (Holland and Powell, 1998) and can yield some incoherences between the pseudosections and what is actually observed in the samples.

To estimate the *P–T* conditions of the metamorphic peak, the compositions of the matrix minerals can be used together with that of the garnet rims since biotite, muscovite and plagioclase are homogeneous (except plagioclase in F13) and since the garnet porphyroblasts do not show any late resorption and/or retrograde reequilibration (Fig. 5). Conventional thermobarometry could be applied but the multi-equilibrium approach, coupled with the use of an internally consistent set of thermodynamic data, is preferred to determine the *P–T* conditions of the metamorphic peak. The reasons of this choice are those stated by Powell and Holland (1994) in their tutorial paper on optimal geothermobarometry. The software THERMOCALC enables to calculate average *P–T* conditions, using an independent set of reactions representing all possible equilibria in the rock and considering the correlations among the reactions used.

Both inverse and forward modelling were conducted with the version 3.21 of THERMOCALC.

4.2. *P–T* pseudosections and garnet nucleation

The six *P–T* pseudosections (Fig. 7) shown in this paper have some common features. First, the garnet (+) boundary labelled g(+) has a curved shape and its position suggests that garnet nucleation should occur at temperatures lower than 480–530 °C in metapelites with chlorite, muscovite, plagioclase and quartz, with or without biotite. Staurolite is present in all pseudosections at temperatures between 540 and 650 °C depending on the pressure, but its stability field is reduced in F13, this rock beeing rather poor in aluminium (Table 2), a feature which is further illustrated by the lack of kyanite in the *P–T* pseudosection. There is no major difference between the pseudosection of the staurolite-bearing sample F24 and most of those calculated for staurolite-free metapelites F6, F7 and F29. No potash feldspar is stable in the six *P–T* pseudosections calculated with an excess of water. A melt appears in all samples, at temperatures higher than about 650 °C.

In order to use the information contained in the garnet zoning, different composition isopleths calculated with THERMOCALC are drawn on the *P–T* pseudosections. This work is made exhaustively only for F4 (Fig. 8). It is remarkable that the lines of equal mole fraction of Mn, nearly parallel to the garnet (+) boundary, cut the X_{Fe}^{g} and X_{Ca}^{g} isopleths at high angles in the stability fields of the assemblages chl–pl–g–mu–q or chl–pl–g–bi–mu–q. Moreover, in these *P–T* domains, Mn contents and, to a lesser extent, Ca contents vary strongly with the *P–T* conditions in a composition range which can be reasonably investigated with microprobe analyses. At higher temperatures, when chlorite has disappeared, the composition isopleths distribution is no more as clear as in the chl–pl–g–mu–q stability field, and Mn and Ca contents become too low to be used in thermobarometry (Fig. 8). The intersection of the three composition isopleths (X_{Fe}^{g}, X_{Ca}^{g} and X_{Mn}^{g}) is therefore only appropriate to estimate the *P–T* conditions of early garnet growth, in the vicinity of the garnet (+) boundary, at rather low temperatures. Isopleths along with their associated uncertainties (uncertainties in activity models and thermodynamic data and uncertainties in chemical compositions obtained with the microprobe) are calculated using THERMOCALC and plotted in Fig. 9 for garnets of the six metapelites. *P–T* conditions for samples F13 and F24 are not well constrained possibly because a partial re-equilibration took place as temperature was increasing, as indicated by rather flat composition profiles (Fig. 4). On the other hand, samples F4, F6, F7 and F29 yield well defined *P–T* conditions, showing that apparent garnet “cores” have recorded different temperatures (between 500 and 565 °C) and different pressures (between 4.5 and 8 kbar), all lying in the chlorite stability field but varying from one sample to the other. Dark grey areas in Fig. 9 and hachured fields in Fig. 7 show these conditions. This variability could be due to the differences in bulk rock compositions (Table 2) causing the garnet (+) boundary to shift in the *P–T* domain as shown by Fig. 7 and Fig. 9 and, consequently, causing the garnet nucleation to occur at different stages of the prograde metamorphism. Different *P–T* conditions of garnet growth could also be explained by different locations of the garnet-bearing metapelites in the TPU and, subsequently, by various shapes of the metamorphic *P–T* paths followed by these rocks. However, it is also of particular note here that the *P–T* conditions given by the intersection of composition isopleths never lie exactly on the boundary of the garnet stability field but inside this stability field. Even if the uncertainty domain of the garnet (+) line given by THERMOCALC is taken into account, most of the *P–T* conditions recorded by garnet cores cannot be considered as those prevailing as garnet

began to grow unless the garnet nucleation requires some overstepping (Stowell et al., 2001). Vance and Mahar (1998) have already observed this phenomenon and they have proposed several hypotheses to explain it: either ilmenite influence on Mn content, or kinetics, or garnet resorption, or diffusional modifications. However, the problem may also originate from a non-centre cut of garnet grains: if the sections were not cut exactly through the garnet cores, the analysed compositions do not correspond to the foremost growth stage and to *P–T* conditions for garnet nucleation. Therefore, isopleths intersections drawn for different garnet crystals cut more or less close to their core could yield various *P–T* conditions corresponding to successive stages in the garnet growth. One could expect that different types of garnet sections could enable to determine several points on the prograde *P–T* path. Unfortunately, as garnet grows, chemical elements are locked into the interior of the grains, causing a shift in the bulk composition of the reacting system, away from the fractionated composition. To evaluate the effects of this bulk composition variation on the location of Ca and Mn contours in a *P–T* pseudosection, a partial *T–X* pseudosection was calculated for F7, at 8 kbar and between 500 and 700 °C (Fig. 10). On the *X*-axis, $X = 0$ corresponds to the actual composition of the garnet-bearing metapelite (F7) (Table 2). $X = 1$ is a modified composition obtained by removing from the bulk composition of the whole rock F7 all the garnet cores out of equilibrium which represent about 10 mol % in the mode of the rock (F7-g). This percentage was chosen after calculations with THERMOCALC showing that, at this pressure, the highest possible mode of garnet is about 11 mol% (Fig. 11). A rough estimation of composition for garnet cores out of equilibrium was done, using data given in Table 3. It appears that the change in composition due to the disequilibrium growth of zoned garnet has no significant effect upon the nature of mineral assemblages since most of the field boundaries are nearly horizontal in the garnet stability field drawn in Fig. 10. On the other hand, the X_{Ca}^{g} and X_{Mn}^{g} contours are oblique with respect to the *X*-axis and, at a fixed *P–T* condition, in the subsolidus domain, the Ca content decreases (X_{Ca}^{g} variation up to − 0.10) and the Mn content increases (X_{Mn}^{g} variation up to + 0.15) as the mode of garnet cores increases. Therefore, for a section cut rather far from the garnet core, it would not be possible to use the Ca and Mn contours plotted on a *P–T* pseudosection calculated for the whole rock as thermobarometric tools.

4.3. Multi-equilibrium thermobarometry and peak *P–T* conditions

Table 8 gives the results of calculations using the "average *P–T*" mode of THERMOCALC 3.21, the activities of the different end-members in garnet rims and matrix minerals being determined previously with the AX-software, a calculation program using simple activity-composition models for natural rock-forming minerals ([Holland and Powell, 1990] and [Holland and Powell, 1998]). Average pressures and temperatures with their uncertainties (+/− 1 sigma) are derived from the independent set of equilibria given for each sample. All the correlation coefficients "*cor*" between the pressures and temperatures are positive and higher than 0.7. Therefore, all uncertainty ellipses (Fig. 9) are moderately flattened and their main axis has a positive slope (Powell and Holland, 1994). For every sample, the diagnostic parameter called "*sigfit*" being lower than the cutoff value given in parentheses for all samples, it can be considered that a solution for *P–T* has been found that is consistent with the input data within their uncertainties. The "*hat*" values delivered by THERMOCALC for each end-member in a given system are not reported in Table 8 but they show that the components grossular and, to a lesser extent, pyrope have a controlling influence on the results.

Multi-equilibrium calculations were realized with the mode "Average-*P–T*" of THERMOCALC 3.21 ([Powell and Holland, 1988] and [Powell and Holland, 1994]). These

results are obtained using the chemical compositions of matrix minerals and garnet rims. The *P* and *T* uncertainties correspond to 1 "*sigma*". The parameters "*cor*" and "*sigfit*" given by THERMOCALC are briefly explained in text.

THERMOCALC yields all peak *P–T* conditions in the range 615–655 °C (+/− 35 °C) and 6.6–9.0 kbar (+/− 1.2 kbar) except for F13 (5.8 +/− 1.2 kbar). All these results are shown graphically (Fig. 7 and Fig. 9) with uncertainty ellipses calculated at the 2 "sigma" level (Worley and Powell, 2000). It appears that the multi-equilibrium approach does not yield precise *P–T* conditions for the metamorphic peak of the TPU in the Quercy area but its results are however very useful to estimate roughly the prograde *P–T* evolution by comparing these peak conditions to *P–T* conditions obtained before for garnet nucleation.

4.4. Prograde *P–T* evolution

The problem is now to determine the *P–T* path between the apparent beginning of garnet growth and the metamorphic peak. Most of the temperatures determined with the garnet core compositions (dark grey areas in Fig. 9 and hachured domains in Fig. 7) are clearly lower than those calculated using the equilibrium between matrix minerals and garnet rims (ellipses in Fig. 9 and Fig. 7). There are however two types of garnets: garnets in F4, F7 and F29, characterized by a Ca-rich core and a Ca-poor rim, have recorded higher temperature increases than garnets in F6, F13 and F24 which have a constant low Ca content (Fig. 4). The change in pressure is not so clear: while samples F4 and F6 show a possible pressure increase from garnet cores to rims, the other samples do not indicate an indisputable pressure evolution. Fortunately, the garnet zonings provide useful evidences to constrain the prograde *P–T* path as shown hereafter.

If the isopleths distribution plotted in the *P–T* pseudosection of F4 (Fig. 8) is generalized to all samples characterized by similar pseudosections (samples F6, F7, F24, F29), Ca zoning of garnets can be used to constrain the prograde *P–T* evolution. In first approximation, the *P–T* paths of garnets in F4, F7 and F29 showing homogeneous Ca-rich cores must remain first nearly parallel to X_{Ca}^{g} contours. However, considering the partial *T–X* pseudosection calculated for F7 (Fig. 10), it appears that, at a fixed *P–T* condition in the subsolidus domain, X_{Ca}^{g} decreases as fractional crystallization of garnet is proceeding. In order to hold the Ca content of garnet cores constant, garnet-bearing metapelites F4, F7 and F29 must therefore follow a *P–T* path with a steeper slope than those of the X_{Ca}^{g} isopleths shown in the *P–T* pseudosections. Then, the Ca decrease towards the garnet rims going together with an impoverishment in Mn indicates a second growth stage as temperature was rising towards the metamorphic peak (Fig. 8). A further constraint on the heating path can be extracted from Ca and Y distribution maps of garnet F7 (Fig. 5) which indicate a resorption stage of the mineral followed by a renewed growth as already emphasized. Since THERMOCALC enables to calculate the modal composition of a rock (in mol %) at a given $P–T–X_{H2O}$ condition, it is possible to show how garnet resorption occurs through mineral reactions for which no obvious evidence exists in the rock, except garnet zoning. The modal composition of F7 was computed for a system just saturated in water, between 500 and 700 °C, at 5, 8 and 10 kbar (Fig. 11). Indeed, at 5 and 8 kbar, staurolite appears with increasing temperature when chlorite begins to breakdown whereas, at 10 kbar, kyanite is the phase nucleating as chlorite disappears. The evolution of the molar proportions of the different phases as temperature increases, in subsolidus conditions, shows clearly that, at 5 and 8 kbar, garnet dissolves to give staurolite before growing again, first slightly so long it coexists with staurolite, then steeply as staurolite disappears. At 10 kbar, garnet goes on growing as kyanite appears and no

garnet resorption is observed at subsolidus temperatures. Therefore, garnet zoning features combined with mode calculations enable to assert that F7, a staurolite-free metapelite, did contain staurolite during the prograde stage of metamorphism, and that the prograde *P–T* path cuts the chlorite(−) boundary in the *P–T* pseudosection at a pressure lower than that of point I (Fig. 7 and Fig. 9), that is lower than about 9.3 kbar. The *P–T* path recorded by the F7 garnet outer ring is therefore likely to correspond to a nearly isobaric heating at about 8.5–9 kbar. Consequently, metapelites F4, F7 and F29 would have followed the same *P–T* path with a first stage corresponding to a burial causing a pressure increase and a moderate temperature increase (constrained by Ca isopleths) followed by a second period corresponding to a nearly isobaric heating (constrained by garnet resorption and peak conditions) occurring as the rocks were reequilibrating at their deepest position in the crust. The burial part of the *P–T* path seems to be recorded more or less completely by the garnets in the three metapelites F4, F7, and F29. The best garnet section, that is probably the closest to the core, is observed in the smallest garnet, in sample F4, and yields the most complete and reliable prograde *P–T* path.

Among the three other garnets, only that of sample F6 can be considered since the uncertainty domains associated with the three isopleths of garnets in F13 and F24 do not intersect (Fig. 9). The information recorded by this garnet in F6 could be in agreement with a pressure and a temperature increase but the low Ca content of the garnet does not enable to further constrain the shape of this *P–T* path which lies at much higher temperatures than those of F4, F7 and F29 for a given pressure.

4.5. Concluding comments on the validity of the results

The *P–T* pseudosections used in order to estimate the *P–T* conditions for garnet nucleation were calculated for water saturated systems. The saturation hypothesis seems reasonable for the following reasons. First, potash feldspar, which does not appear on the *T–X* pseudosection (Fig. 10) and which crystallizes only under water-absent conditions after calculated $T–X_{H2O}$ pseudosections (not shown in this paper), is not observed in the six metapelites. These facts are compatible with the presence of free water during metamorphism. Then, even under water saturation, peak conditions (Fig. 7) are mostly at lower temperatures than the solidus curves which are only slightly affected by disequilibrium growth of zoned garnet (Fig. 10). These observations are not at variance with the lack of anatexis in the natural samples.

The use of garnet isopleths as a thermobarometric tool (Fig. 9) is satisfying as long as their associated uncertainty domains are thin enough and intersect in the vicinity of the garnet (+) boundary; it is especially the case for the garnet core in F4. If overstepping of garnet nucleation is large enough, even the garnet core composition in F6 can be used. Then, Ca isopleths can help to constrain the first stage of the prograde *P–T* path if the Ca contents are higher than about 0.10 so that the Ca contours are located in the *P–T* field where the isopleths distribution is appropriate for thermobarometry (Fig. 8); it is the case for garnet cores in F4, F7 and F29 (Table 3). The most reliable prograde path is therefore that for sample F4. Finally, considering the "*hat*" values given by THERMOCALC (Powell and Holland, 1994), the *P–T* conditions of the metamorphic peak are strongly dependent on the grossular and pyrope contents of garnet rims. This can be a problem because the Ca contents of the rims are rather low ($X_{Ca}^{g} < 0.09$) and, consequently, the analytical uncertainties can be important.

The last point to consider in this discussion is the fact that the stability fields of observed natural parageneses coincide partly with the uncertainty ellipses corresponding to the *P–T* peak conditions only for samples F4, F13 and F24 (stippled fields in Fig. 7). In metapelites

F6, F7 and F29, there is one phase missing in the natural mineral assemblages compared to the pseudosections. This phase could be either chlorite, or staurolite or kyanite. If sample F7 is considered, the garnet zoning shows that staurolite has already disappeared (discussion in Section 4.4). Therefore, the only possibility is that kyanite is missing in the natural samples. Mode calculations (Fig. 11) show that kyanite, which appears at the expense of staurolite at 8 kbar or of chlorite at 10 kbar, is not abundant at all (less than 2.3 mol%). It is therefore possible that not enough thin sections were studied to be able to observe kyanite. The fact that kyanite is not present in sample F7 could also be explained by kinetics if nucleation conditions must be overstepped by some considerable degree.

Very fortunately, even if a few questions remain without answer in this thermobarometric investigation of six metapelites sampled in the TPU, the garnet zoning gives enough information about the shape of the *P–T* path to be sure that the TPU in the Quercy area has undergone an increase in pressure (F4) followed by a nearly isobaric heating (F4, F29, F7).

5. Discussion and conclusion

5.1. A compressive heating tectonic setting for the TPU in Quercy

This study provides the first quantitative thermobarometric data on the *P–T* evolution of the uppermost TPU in the French Massif Central. In the Quercy area, the structural data show that the micaschists experienced only the D2 tectono-metamorphic event. The thermobarometric results support a clockwise prograde metamorphic *P–T* path ending with an isobaric heating. The peak conditions correspond to the amphibolite facies conditions (615–655 °C +/− 35 °C and 6.6–9.0 +/− 1.2 kbar for most of the samples). Such a compressional heating path is coeval with the top-to-the NW D2 shearing associated to the superposition of the TPU upon the UGU. In spite of the lack of quantitative *P–T* data from the underlying gneiss units, the kyanite–staurolite–garnet assemblages described there ([Feix, 1988] and [Guillot et al., 1992]) would suggest that there are neither significant temperature nor pressure gaps between the two units during the D2 event. Furthermore, a recent thermobarometric study, about 100 km farther on to the north, has shown that temperatures calculated in the footwall (UGU and LGU) are slightly lower than those of the TPU (Bellot, 2001). Thus, the *P–T* path experienced by the TPU in the Quercy area complies with a burial event rather than with a syn-orogenic denudation setting.

5.2. Consequence for the geodynamics of the Variscan Belt

The top-to-the NW D2 shearing observed in the TPU is also widely represented in the underlying units of the French Massif Central. This D2 event occurs after a top-to-the SW D1 event during which the UGU, including the exhumed eclogitic relics, overthrusts the LGU ([Burg et al., 1984], [Faure et al., 1997], [Roig and Faure, 2000], [Faure et al., 2004] and [Faure et al., 2005]). The D1 event is dated at *ca.* 385–375 Ma by several radiometric methods, namely Rb–Sr on whole rock, chemical U–Th/Pb on monazite and $^{40}Ar/^{39}Ar$ on amphibole ([Costa, 1992], [Boutin and Montigny, 1993], [Duthou et al., 1994] and [Bé Mézème, 2005]).

In contrast to other TPU areas where the D1 event is not documented, in the Rouergue area (Fig. 1a), the Saint–Sernin–sur–Rance Nappe underwent a polyphase tectonic history. There, it can be shown that during D1, the Saint–Sernin–sur–Rance Nappe was overthrust by the

LGU and UGU with a top-to-the SW displacement. Then during D2, the whole stack was overturned and sheared to the NW. The early D1 structures, such as stretching lineation and intrafolial folds, were deformed again, and a new NW–SE trending mineral and stretching lineation developed ([Duguet and Faure, 2004a] and [Duguet and Faure, 2004b]). The allochthonous character of the TPU in South Limousin is supported by seismic profiles (Bitri et al., 1999), but the tectonic significance of the *ca.* 360 Ma top-to-the NW D2 is not yet well understood (Faure et al., 1997). Our thermobarometric data support a model in which crustal thickening and thermal input are coeval with top-to-the NW shearing. This leads us to discard the interpretation of the top-to-the NW shearing as resulting of syn-orogenic extension (Mattauer et al., 1988).

In the case of compressional tectonic setting for the D2 event, several models need to be discussed. Brun and Burg (1982) suggested that the Barrovian metamorphism during the top-to-the NW D2 event was the consequence of the evolution of continental collision between Armorica and Gondwana. After the D1 thrust loading, contemporaneous with top-to-the SW shearing, large intracontinental transcurrent shear zones played a significant role and reworked the previous stack of nappes. The horizontal movements became parallel to the continental blocks boundaries and the tectonic framework changed into a tranpressional context in which thrusting was subordinate to wrenching. In the Massif Armoricain, recent studies combining seismic profiles and gravimetric modelling have shown that top-to-the NW displacement would be coeval with the major dextral shearing of the South Armorican Shear Zone ([Bitri et al., 2003] and [Martelet et al., 2004]). Such a structure would be similar to a "pop-up structure" (*e.g.* [Richard, 1991] and [McClay and Bonora, 2001]).

Nevertheless, the explanation of such a progressive evolution in terms of a monocyclic model does not take into account other data among which the most important one is the Late Devonian rifting observed in several parts of the French Variscan Belt (Faure et al., 1997). In the French Massif Central, several lines of evidence argue for an Upper Devonian arc-back arc setting. For instance, in the NE Massif Central, the Brévenne area is presently interpreted as a Late Devonian oceanic basin opened within an already metamorphic basement and closed through top-to-the NW ductile and synmetamorphic shearing (Leloix et al., 1999). In the South Limousin area, Doubinger and Guillot (1971) have described an assemblage of un-metamorphosed gabbro, dolerite, basalt, chert and Devonian limestone that overlies the TPU. These rocks are interpreted as relics of an ophiolitic nappe overthrust upon the TPU ([Guillot, 1981], [Floc'h, 1983], [Girardeau et al., 1986] and [Ledru et al., 1989]). These observations have led some authors to consider that the top-to-the NW event is related to the closure of limited oceanic domains. Thus, the Variscan orogeny can be seen as the superposition of two orogenic cycles ([Faure et al., 1997], [Pin and Paquette, 2002] and [Faure et al., 2005]). The present data suggest that burial and top-to-the NW thrusting took place under a moderate to high geothermal gradient during magmatic activity (35–40 °C km^{-1}). This scheme would be very similar to that presented by Whitney et al. (1999) for the Canadian Cordillera where thickening is coeval with magmatism during sub-horizontal arc contraction. The burial and metamorphism of the TPU might be the result of the closure of limited oceanic domain further south followed by intra-arc contraction processes. The present state of knowledge does not allow to propose a comprehensive geodynamic interpretation.

Acknowledgements

We acknowledge financial support from the French Geological Survey B.R.G.M. We thank O. Rouer who performed X-ray composition maps, J. Boissonnas for assistance with some English problems, J.-M. Lardeaux, St. Guillot and D. Robinson for providing helpful comments on an early draft of this paper, and I. Buick and two anonymous reviewers for suggestions that significantly improved the manuscript. N. Le Breton attended to the THERMOCALC Workshop in Pavia in 2002 and is greatly indebted to R. Powell for his communicative enthusiasm.

References

Bé Mézème, 2005 Bé Mézème, E., 2005. Application des méthodes de datation ponctuelle et *in situ* à la fusion crustale dans la chaîne hercynienne. Thèse de Doctorat, Université d'Orléans, France, 300 pp.

Bellot, 2001 Bellot, J.-P., 2001. La structure de la croûte varisque du Sud-Limousin (Massif Central Français) et ses relations avec les minéralisations aurifères tardi-orogéniques : apport des données géologiques, gîtologiques, géophysiques et de la modélisation 3D. Thèse de Doctorat, Université Montpellier, France, 320 pp.

Bitri et al., 1999 A. Bitri, C. Truffert, J.-P. Bellot, V. Bouchot, P. Ledru, J.-P. Milesi and J.-Y. Roig, Imagerie des paléochamps hydrothermaux As–Au–Sb d'échelle crustale et des pièges associés dans la chaîne varisque : sismique réflexion verticale (GéoFrance 3D : Massif Central français), *Comptes Rendus de l'Académie des Sciences de Paris* **329** (1999), pp. 771–777.

A. Bitri, M. Ballèvre, J.-P. Brun, J. Chantraine, D. Gapais, P. Guennoc, C. Gumiaux and C. Truffert, Seismic imaging of the Hercynian collision zone in the south-eastern Armorican Massif (Armor 2 project/Géofrance 3D Program), *Comptes Rendus Géosciences* **335** (2003), pp. 969–979.

Bouchez and Jover, 1986 J.-L. Bouchez and O. Jover, Le Massif Central : un chevauchement de type himalayen vers l'ouest — nord-ouest, *Comptes Rendus de l'Académie des Sciences de Paris* **302** (1986), pp. 675–680.

Boutin and Montigny, 1993 R. Boutin and R. Montigny, Datation $^{39}Ar/^{40}Ar$ des amphibolites du complexe leptyno-amphibolique du plateau d'Aigurande: collision varisque à 390 Ma dans le nord-ouest du Massif Central français, *Comptes Rendus de l'Académie des Sciences de Paris* **316** (1993), pp. 1391–1398.

Brun and Burg, 1982 J.-P. Brun and J.-P. Burg, Combined thrusting and wrenching in the Ibero–Armorican arc: a corner effect during continental collision, *Earth and Planetary Science Letters* **6** (1982), pp. 319–332.

Burg et al., 1984 J.-P. Burg, A. Leyreloup, J. Marchand and P. Matte, Inverted metamorphic zonation and large scale thrusting in the Variscan Belt: an example in the French Massif

Central. In: D.H.W. Hutton and D.J. Sanderson, Editors, *Variscan tectonics of the North Atlantic region*, *Special Publication of the Geological Society of London* (1984), pp. 44–61.

Costa, 1992 S. Costa, East–West diachronism of the collisional age in French Massif Central: implications for the European Variscan orogen, *Geodinamica Acta* **5** (1992), pp. 51–68.

Doubinger and Guillot, 1971 J. Doubinger and P.-L. Guillot, Découverte d'Acritarches dans les schistes sériciteux de Génis (Dordogne), *Comptes Rendus de l'Académie des Sciences de Paris* **272** (1971), pp. 2763–2764.

Duguet and Faure, 2004a M. Duguet and M. Faure, Granitoid emplacement during a thrusting event: structural analysis, microtextural evidences and quartz *c*-axis patterns. An example from Hercynian plutons in the French Massif Central, *Journal of Structural Geology* **26** (2004), pp. 927–945.

Duguet and Faure, 2004b M. Duguet and M. Faure, Successive shearing tectonics during the Hercynian collisional evolution of the southwestern French Massif Central, *Bulletin de la Société Géologique de France* **175** (2004), pp. 49–59.

Duthou et al., 1994 J.-L. Duthou, M. Chenevoy and M. Gay, Age Rb-Sr Dévonien moyen des migmatites à cordiérite des Monts du Lyonnais (Massif Central Français), *Comptes Rendus de l'Académie des Sciences de Paris* **319** (1994), pp. 791–796.

Faure, 1995 M. Faure, Late Carboniferous extension in the Variscan French Massif Central, *Tectonics* **14** (1995), pp. 132–153.

Faure et al., 1997 M. Faure, C. Leloix and J.-Y. Roig, L'évolution polycyclique de la chaîne hercynienne, *Bulletin de la Société Géologique de France* **168** (1997), pp. 695–705.

Faure et al., 2004 M. Faure, P. Ledru, J.-M. Lardeaux and P. Matte, Paleozoic orogenies in the French Massif Central. A cross section from Bézier to Lyon, *32nd International Geological Congress in Florence (Italy)*, *Field Trip Guide Book* **vol. B22** (2004) 40 pp., freely downloadable in http://www.apat.gov.it/site/it-IT/APAT/FieldtripGuidebooks/Pre-Congress_Field_Trips/..

Faure et al., 2005 M. Faure, E. Bé Mézème, M. Duguet, C. Cartier and J. Talbot, Paleozoic tectonic evolution of medio-europa from the example of the French Massif Central and Massif Armoricain. In: R. Carosi, R. Dias, D. Iacopini and G. Rosenbaum, Editors, *The southern Variscan Belt*, *Journal of the Virtual Explorer*, *Electronic Edition* **vol. 19, paper 5** (2005), pp. 1–24.

Feix, 1988 Feix, I., 1988. Etude géologique dans le Sud-Millevaches : lithologie, géochimie, métamorphisme et structure des séries situées au sud de la vallée de la Dordogne. Place dans le Massif Central français occidental. Thèse de 3ème cycle, Université d'Orléans, France, 534 pp.

Floc'h, 1983 Floc'h, J.-P., 1983. La série métamorphique du Limousin Central. Thèse d'Etat, Université de Limoges, France, 444 pp.

Girardeau et al., 1986 J. Girardeau, G. Dubuisson and J.-C. Mercier, Cinématique de mise en place des ophiolites et nappes cristallophylliennes du Limousin, ouest du Massif Central français, *Bulletin de la Société Géologique de France* **8** (1986), pp. 849–860.

Guillot, 1981 Guillot, P.-L., 1981. Les séries métamorphiques du Bas Limousin : de la vallée de l'Isle à la vallée de la Vézère, le socle en bordure du Bassin aquitain. Thèse d'état, Université d'Orléans, France, 391 pp.

Guillot et al., 1989 P.-L. Guillot, A. Lefavrais-Raymond, J.-G. Astruc and D. Bonijoly, Notice de la carte géologique au 1/50000: Feuille de Lacapelle Marival (834), B.R.G.M, Orléans, France (1989) 67 pp..

Guillot et al., 1992 P.-L. Guillot, J.-G. Astruc, I. Feix, L. Humbert, M. Lefavrais-Henri, A. Lefavrais-Raymond, A. Michard, G. Monier and P. Roubichou, Notice de la carte géologique au 1/50000: Feuille de Saint-Céré (810), B.R.G.M, Orléans, France (1992) 76 pp..

Holland and Powell, 1990 T.J.B. Holland and R. Powell, An enlarged and updated internally consistent thermodynamic dataset with uncertainties and correlations: the system K_2O–Na_2O–CaO–MgO–MnO–FeO–Fe_2O_3–Al_2O_3–TiO_2–SiO_2–C–H_2–O_2, *Journal of Metamorphic Geology* **8** (1990), pp. 89–124.

Holland and Powell, 1998 T.J.B. Holland and R. Powell, An internally consistent thermodynamic data set for phases of petrological interest, *Journal of Metamorphic Geology* **16** (1998), pp. 309–343

Hollister, 1966 L.S. Hollister, Garnet zoning: an interpretation based upon the Rayleigh fractionation model, *Science* **154** (1966), pp. 1647–1651.

Ledru et al., 1989 P. Ledru, J.-M. Lardeaux, D. Santallier, A. Autran, J.-M. Quenardel, J.-P. Floc'h, G. Lerouge, N. Maillet, J. Marchand and A. Ploquin, Où sont les nappes dans le Massif Central français?, *Bulletin de la Société Géologique de France* **8** (1989), pp. 605–618.

Leloix et al., 1999 C. Leloix, M. Faure and J.-L. Feybesse, Hercynian polyphase tectonics in the northeast French Massif central: the closure of the Brévenne Devonian-Dinantian rift, *International Journal of Earth Sicences* **88** (1999), pp. 409–421.

McClay and Bonora, 2001 K. McClay and M. Bonora, Analog models of restraining stepovers in strike-slip fault systems, *Association of American Petroleum Geology Bulletin* **85** (2001), pp. 233–260.

Martelet et al., 2004 G. Martelet, P. Calcagno, C. Gumiaux, C. Truffert, A. Bitri, D. Gapais and J.-P. Brun, Integrated 3D geophysical and geological modelling of the Hercynian Suture Zone in the Champtoceaux area (south Brittany, France), *Tectonophysics* **382** (2004), pp. 117–128.

Mattauer et al., 1988 M. Mattauer, M. Brunel and P. Matte, Failles normales ductiles et grands chevauchements. Une nouvelle analogie entre l'Himalaya et la chaîne hercynienne du Massif Central français, *Comptes Rendus de l'Académie des Sciences de Paris* **306** (1988), pp. 671–676

Matte, 1991 P. Matte, Accretionary history and crustal evolution of the Variscan Belt in Western Europe, *Tectonophysic* **196** (1991), pp. 309–337.

Pin and Paquette, 2002 C. Pin and J.-L. Paquette, Le magmatisme basique calcoalcalin d'âge dévono-dinantien du nord du Massif Central, témoin d'une marge active hercynienne: arguments géochimiques et isotopiques Sr/Nd, *Geodinamica Acta* **15** (2002), pp. 63–77.

Powell and Holland, 1988 R. Powell and T.J.B. Holland, An internally consistent thermodynamic dataset with uncertainties and correlations: 3: application, methods, worked examples and a computer program, *Journal of Metamorphic Geology* **6** (1988), pp. 173–204.

Powell and Holland, 1994 R. Powell and T.J.B. Holland, Optimal geothermometry and geobarometry, *American Mineralogist* **79** (1994), pp. 120–133.

Pyle and Spear, 1999 J.M. Pyle and F.S. Spear, Yttrium zoning in garnet: coupling of major and accessory phases during metamorphic reactions, *Geological Materials Research* **1** (1999), pp. 1–49.

Richard, 1991 P.D. Richard, Experiments on faulting in a two layer cover sequence overlying a reactivated basement fault with oblique (normal wrench or reverse wrench) slip, *Journal of Structural Geology* **13** (1991), pp. 459–469.

Roig and Faure, 2000 J.-Y. Roig and M. Faure, La tectonique cisaillante polyphasée du Sud Limousin (Massif Central Français) et son interprétation dans un modèle d'évolution polycyclique de la Chaîne hercynienne, *Bulletin de la Société Géologique de France* **171** (2000), pp. 295–307

Roig et al, 1996 J.-Y. Roig, M. Faure and P. Ledru, Polyphase wrench tectonics in the southern French Massif Central. Kinematic inferences from pre- and syn-kinematic granitoids, *Geologische Rundschau* **85** (1996), pp. 138–153.

Roig et al, 2002 J.-Y. Roig, M. Faure and H. Maluski, Superimposed tectonic and hydrothermal events during the late-orogenic extension in the Western French Massif Central: a structural and $^{40}Ar/^{39}Ar$ study, *Terra Nova* **14** (2002), pp. 25–32.

Santallier and Floc'h, 1989 D. Santallier and J.-P. Floc'h, Tectonique tangentielle et décrochements ductiles dévono–carbonifères superposés dans la région de Bellac (nord–ouest du Massif Central français), *Comptes Rendus de l'Académie des Sciences de Paris* **309** (1989), pp. 1419–1424.

Spear et al., 1990 F.S. Spear, M.J. Kohn, F. Florence and T. Menard, A model for garnet and plagioclase growth in pelitic schists: implications for thermobarometry and P–T path determinations, *Journal of Metamorphic Geology* **8** (1990), pp. 683–696

Stowell and Tinkham, 2003 H.H. Stowell and D.K. Tinkham, Integration of phase equilibria modelling and garnet Sm–Nd chronology for construction of P–T–t paths: examples from the Cordilleran Coast Plutonic Complex, USA. In: D. Vance, W. Muller and I.M. Villa, Editors, *Geochronology: linking the isotopic record with petrology and textures,Special Publication of the Geological Society of London* **vol. 220** (2003), pp. 119–145.

Stowell et al., 2001 H.H. Stowell, D.L. Taylor, D.L. Tinkham, S.A. Goldberg and K.A. Ouderkirk, Contact metamorphic *P–T–t* paths from Sm–Nd garnet ages, phase equilibria modelling and thermobarometry: Garnet Ledge, south-eastern Alaska, USA, *Journal of Metamorphic Geology* **19** (6) (2001), pp. 645–660.

Tinkham et al., 2001 D.K. Tinkham, C.A. Zuluaga and H.H. Stowell, Metapelite phase equilibria modelling in MnNCKFMASH: the effect of variable Al_2O_3 and MgO/(MgO + FeO) on mineral stability, *Geological Materials Research* **3** (2001), pp. 1–42.

Vance and Mahar, 1998 D. Vance and E. Mahar, Pressure-temperature paths from P–T pseudosections and zoned garnets: potential, limitations and examples from the Zanskar Himalaya, NW India, *Contribution to Mineralogy and Petrology* **132** (1998), pp. 225–245.

Whitney et al., 1999 D.L. Whitney, R.B. Miller and S.R. Paterson, P–T–t evidence for mechanisms of vertical tectonic motion in a contractional orogen: northwestern US and Canadian Cordillera, *Journal of Metamorphic Geology* **17** (1999), pp. 75–90.

Worley and Powell, 2000 B. Worley and R. Powell, High-precision relative thermobarometry: theory and a worked example, *Journal of Metamorphic Geology* **18** (2000), pp. 91–101.

Yang and Rivers, 2002 P. Yang and T. Rivers, The origin of Mn and Y annuli in garnet and the thermal dependence of P in garnet and Y in apatite in calc-pelite and pelite, Gagnon terrane, western Labrador, *Geological Materials Research* **4** (2002), pp. 1–35.

Figures

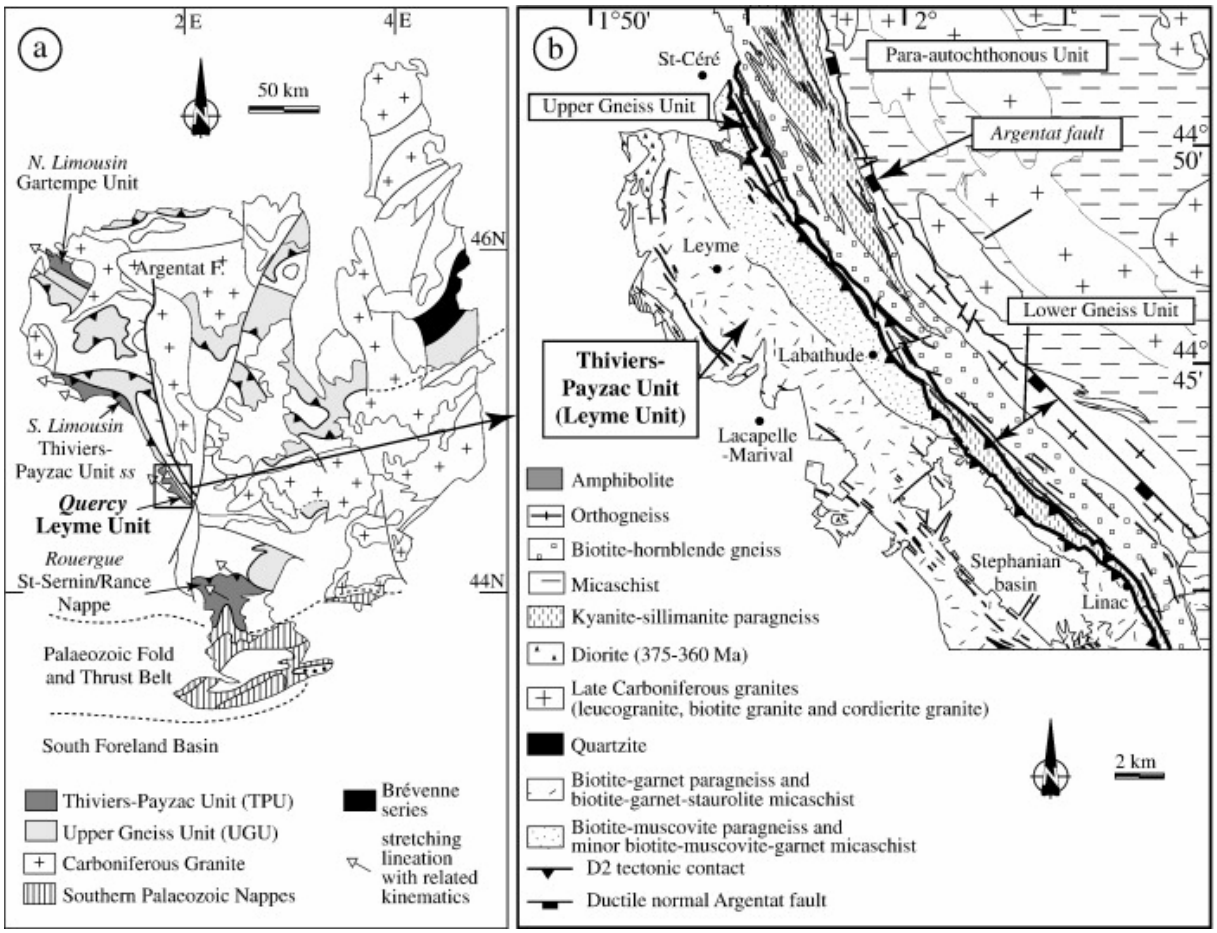

Fig. 1. (a) Structural map of the French Massif Central (simplified from [Ledru et al., 1989] and [Faure et al., 2005]). In the southwestern part of the French Massif Central, the Thiviers-Payzac Unit (TPU) is recognized under different names depending on the area (written in italics). (b) Geological map of the Thiviers-Payzac Unit, locally called Leyme Unit ([Guillot et al., 1989] and [Guillot et al., 1992]) in the Quercy area.

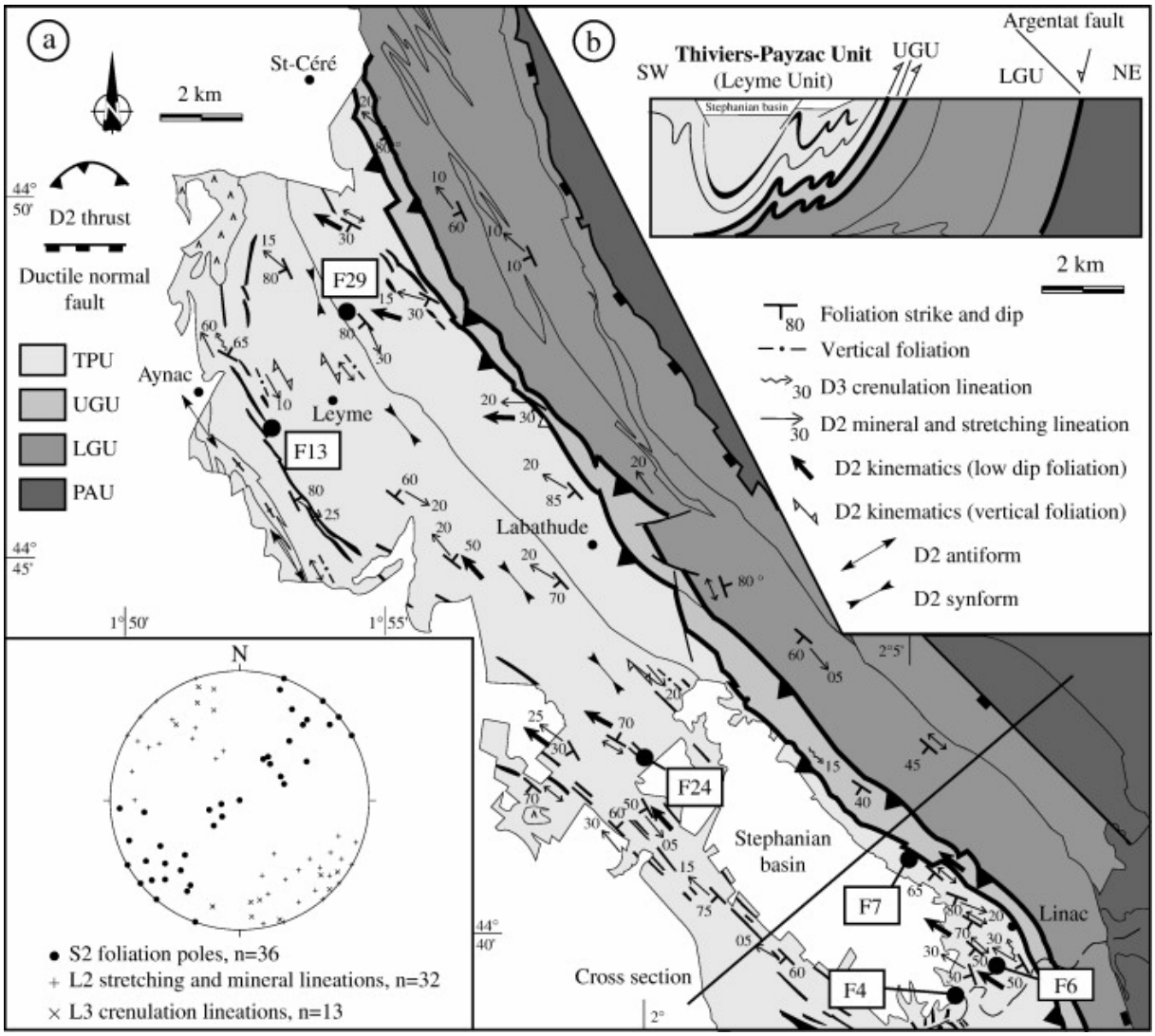

Fig. 2. (a) Structural and kinematic map of the Thiviers-Payzac Unit (TPU) and underlying units (Upper Gneiss Unit: UGU — Lower Gneiss Unit: LGU — Para-autochthonous Unit: PAU) in the Quercy area with sample location of garnet-bearing metapelites used for thermobarometry. (b) Cross section of the study area showing the stack of allochthonous sheets: Thiviers-Payzac Unit (TPU), the Upper Gneiss Unit (UGU) and the Lower Gneiss Unit (LGU) from top to bottom.

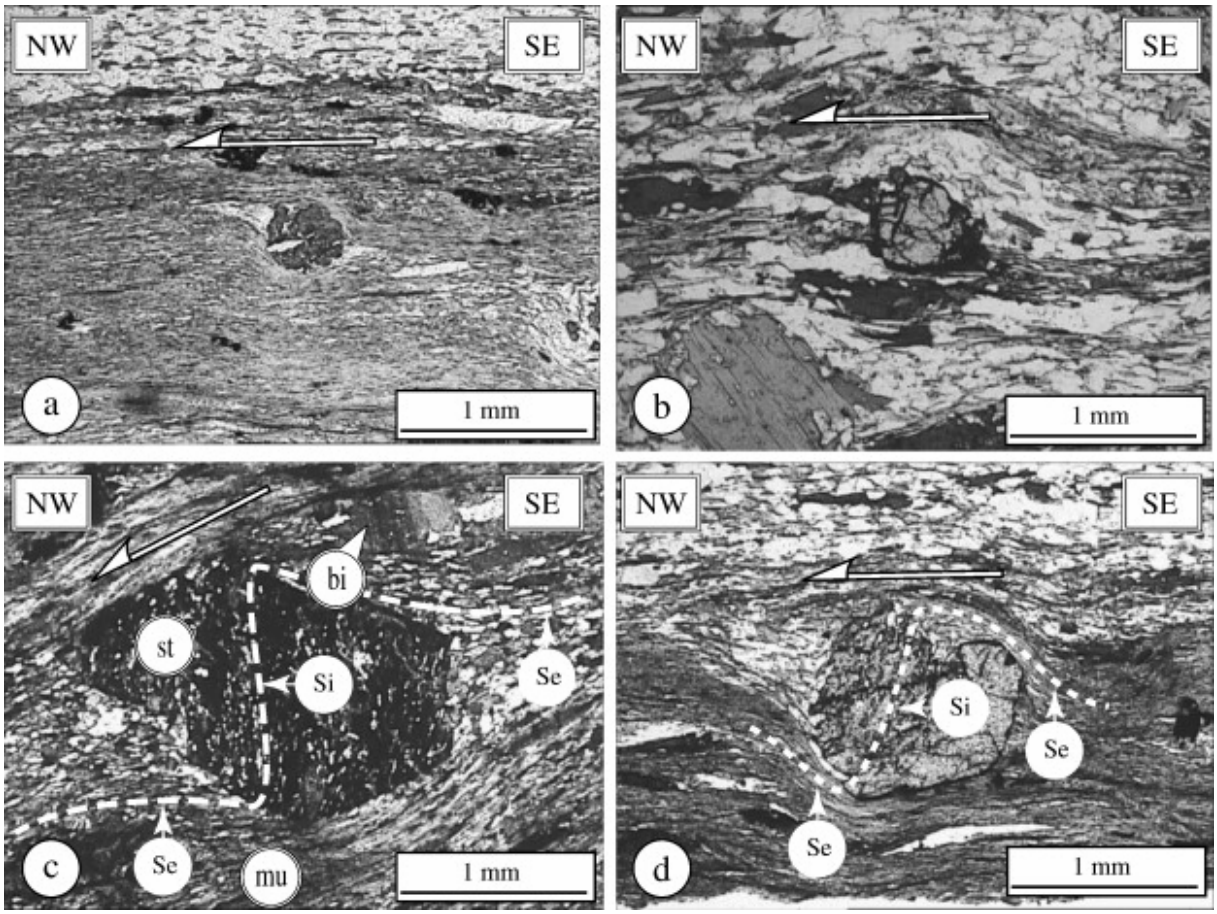

Fig. 3. Optical photomicrographs showing deformation in the Leyme micaschists belonging to the TPU. (a) Assymetric crystallization tail of quartz around garnet giving a top-to-the NW shearing (contact between the TPU and the LGU). (b) Assymetric crystallization tail of biotite around garnet giving a top-to-the NW shearing. (c) Sigmoidal inclusions in a staurolite poikiloblast giving a top-to-the NW shearing (crossed-polarized light). (d) Sigmoidal inclusions in a garnet porphyroblast giving a top-to-the NW shearing (contact between the TPU and the LGU). On (c) and (d), the white dashed line shows the internal (Si) and external (Se) foliations.

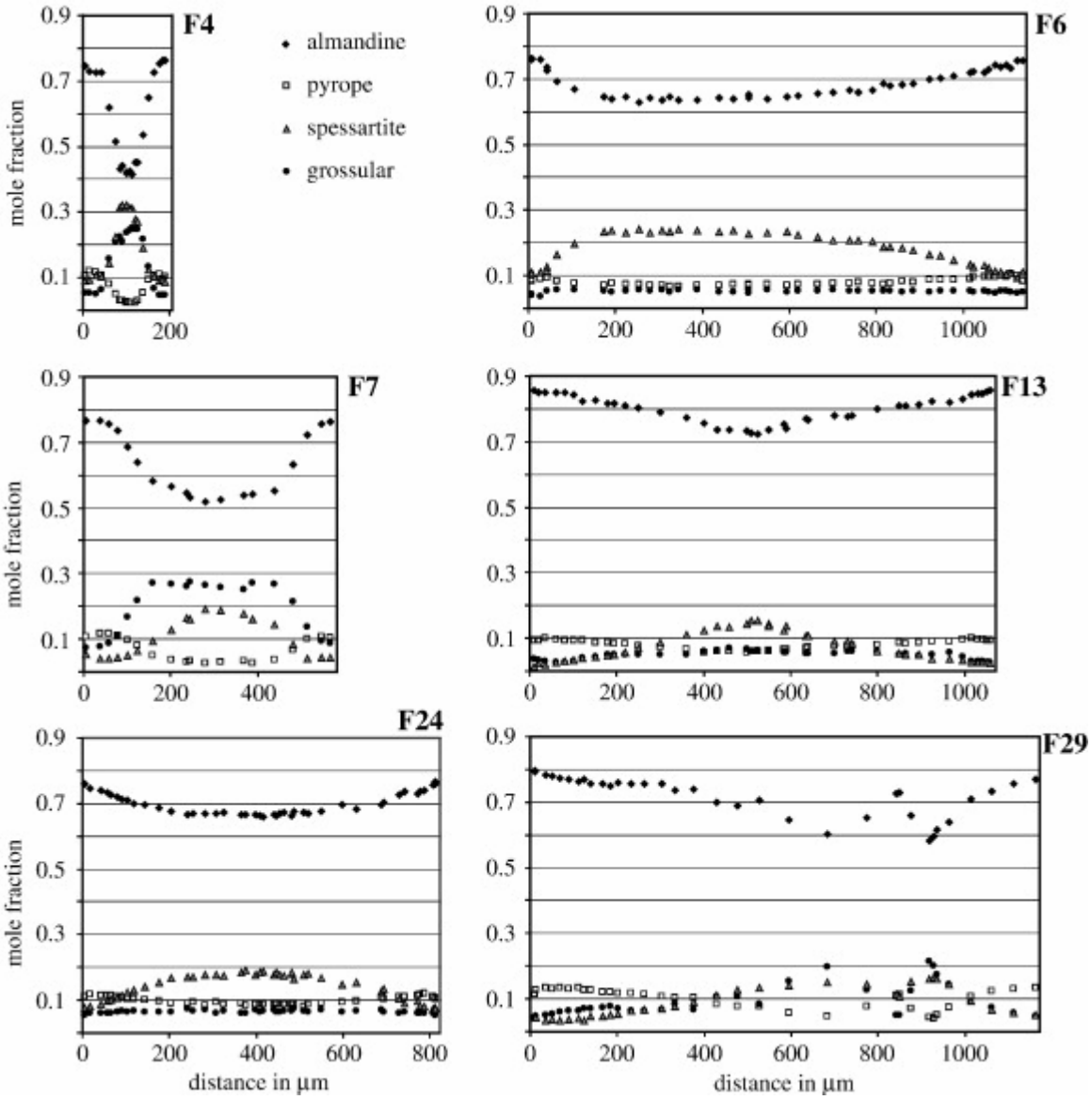

Fig. 4. Zoning profiles of garnet porphyroblasts from metapelites of the TPU (Leyme Unit). The garnet F29 is characterized by two cores corresponding to two nuclei which further grew to form a single grain.

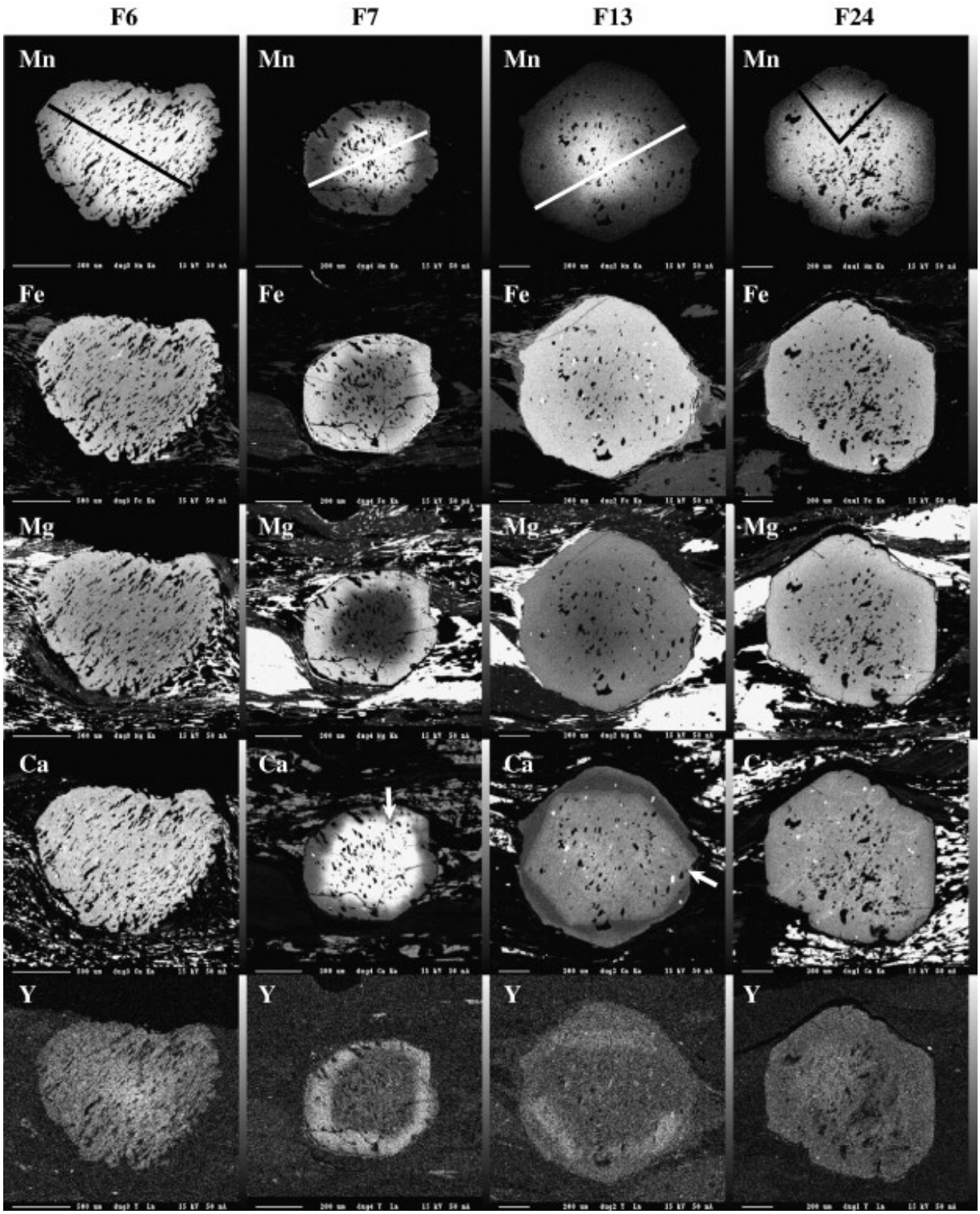

Fig. 5. X-ray element maps for Mn, Fe, Mg, Ca and Y of four garnet porphyroblasts from metapelites (F6, F7, F13 and F24) of the TPU (Leyme Unit). The location of the profiles plotted in Fig. 4 is shown on the Mn distribution maps. On Ca maps for samples F7 and F13, arrows indicate special points discussed in text.

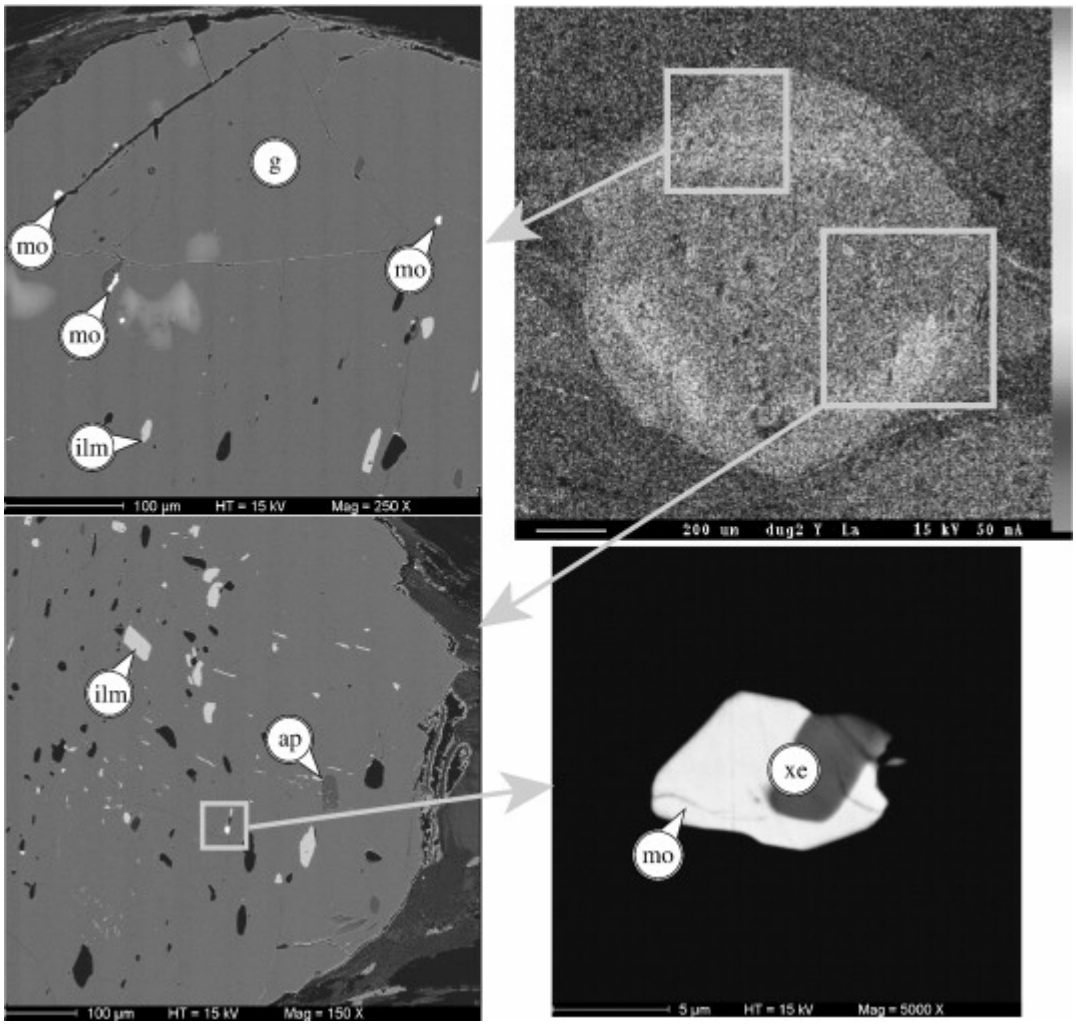

Fig. 6. Textural relationships between monazite and Y zoning in garnet of sample F13. In garnet porphyroblasts, monazite, often enclosing xenotime, is closed to or in the Y-rich annuli.

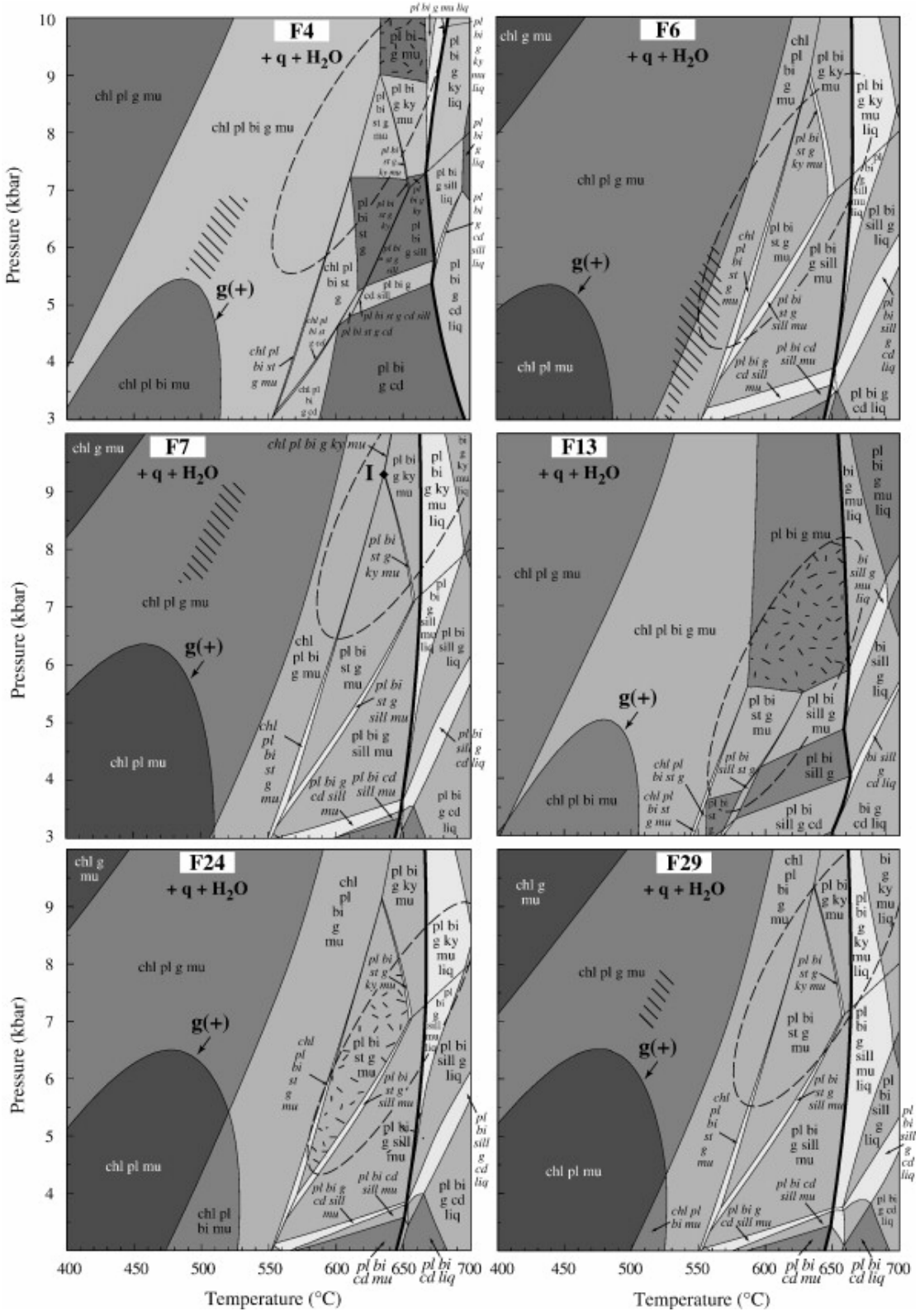

Fig. 7. *P–T* pseudosections calculated with THERMOCALC 3.21 for six metapelites of the TPU (Leyme Unit). The compositions used for computation are given in Table 2, in the reduced model system MnNCKFMA, quartz and water being in excess. The thick solid lines at about 650 °C are the solidus curves. Garnet appears on the curves labelled g(+). The ellipses give the *P–T* conditions of the metamorphic peaks calculated with THERMOCALC (Table 8). The hachured domains correspond to the *P–T* conditions recorded by garnet cores (Fig. 9). Point I indicates the highest possible pressure suffered by the rock F7 (see discussion in Section 4.4). Stippled fields show, when it is possible, the intersections between the *P–T* stability domains of the natural peak parageneses and the uncertainty ellipses giving the peak conditions.

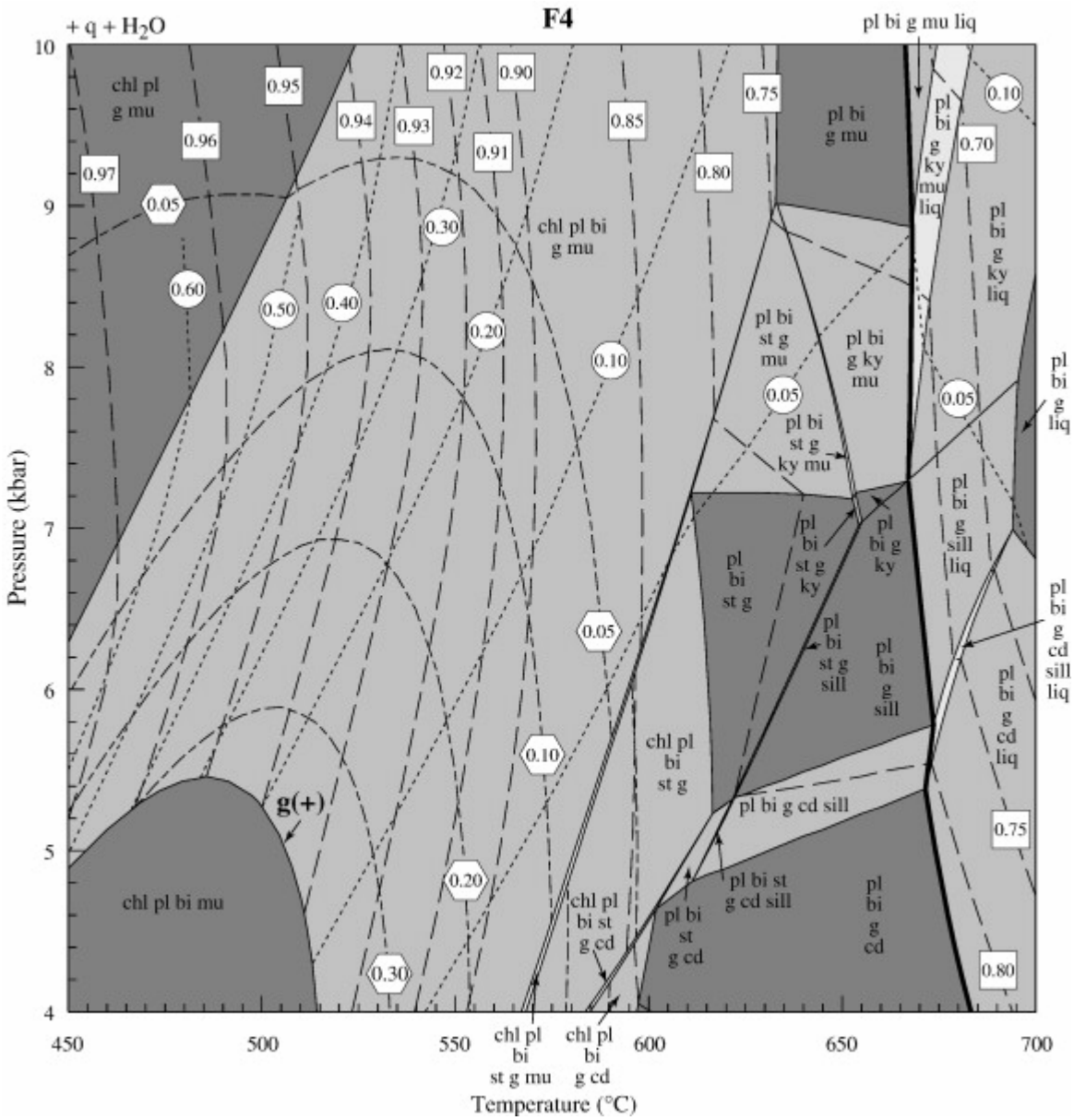

Fig. 8. *P*–*T* pseudosection calculated with THERMOCALC 3.21 for sample F4 as in Fig. 7 but with additional data for garnet composition: dashed lines correspond to the isopleths of Fe, Ca and Mn in garnet (squares: X_{Fe}^{g} = Fe/(Fe + Mg); circles: X_{Ca}^{g} = Ca/(Ca + Fe + Mg + Mn); hexagons: X_{Mn}^{g} = Mn/(Ca + Fe + Mg + Mn)).

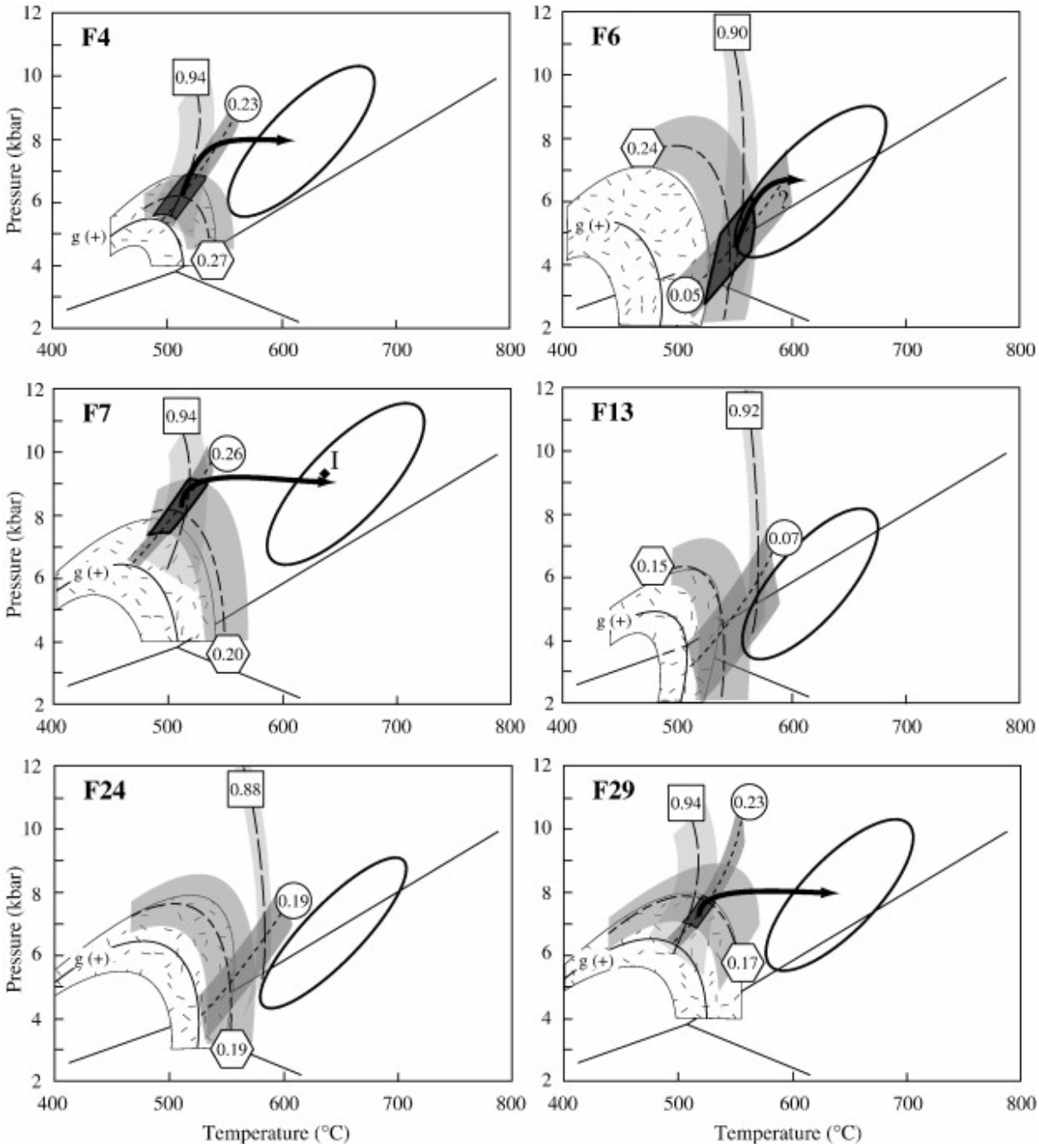

Fig. 9. Results of thermobarometry for six garnet metapelites of the TPU (Leyme Unit). The 2 "sigma" uncertainty ellipses correspond to *P–T* conditions estimated for the metamorphic peak with the "Average *P–T*" mode of THERMOCLAC 3.21 using matrix minerals and garnet rims (Table 8). The uncertainty domain of the g(+) curve is shown with a dashed area. The composition of each garnet core is modelled with three isopleths and their associated uncertainty domains (squares: Fe/(Fe + Mg); circles: Ca/(Ca + Fe + Mg + Mn); hexagons: Mn/(Ca + Fe + Mg + Mn)). The dark grey areas indicate, when possible, the *P–T* conditions recorded by garnet cores. Point I shows the highest possible pressure suffered by the rock F7 (see discussion in section 4.4.). Arrows represent possible prograde *P–T* paths deduced from thermobarometry and from Ca and Mn isopleths.

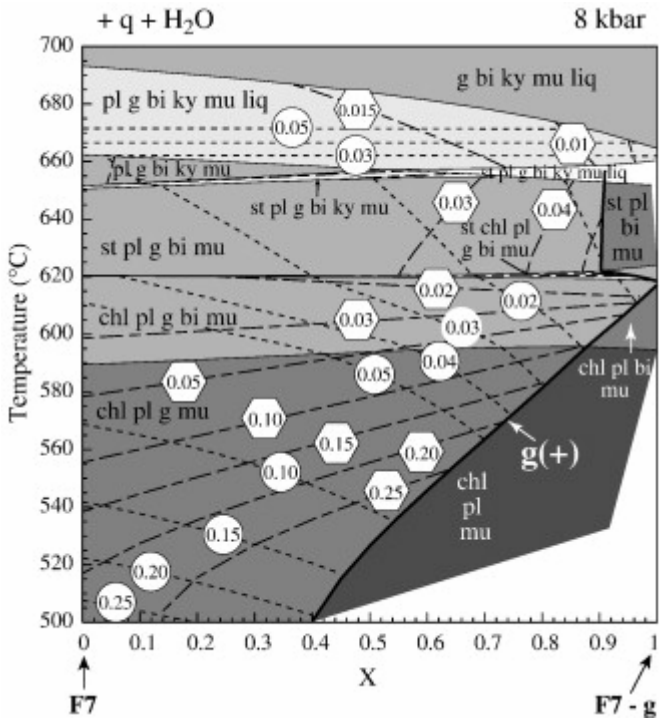

Fig. 10. Partial *T*–*X* pseudosection calculated with THERMOCALC 3.21 with quartz and water in excess. $X = 0$ corresponds to the composition of F7 in model system MnNCKFMA (Table 2) and $X = 1$ represents a modified composition (MnO:0.00, Na_2O:13.02, CaO:0.45, K_2O:9.92, FeO:3.02, MgO:15.62, Al_2O_3:47.26) obtained by removing a roughly estimated garnet core composition from the composition of F7. Dashed lines correspond to the isopleths of Ca and Mn in garnet (circles: Ca/(Ca + Fe + Mg + Mn); hexagons: Mn/(Ca + Fe + Mg + Mn)). The garnet boundary is labelled g(+).

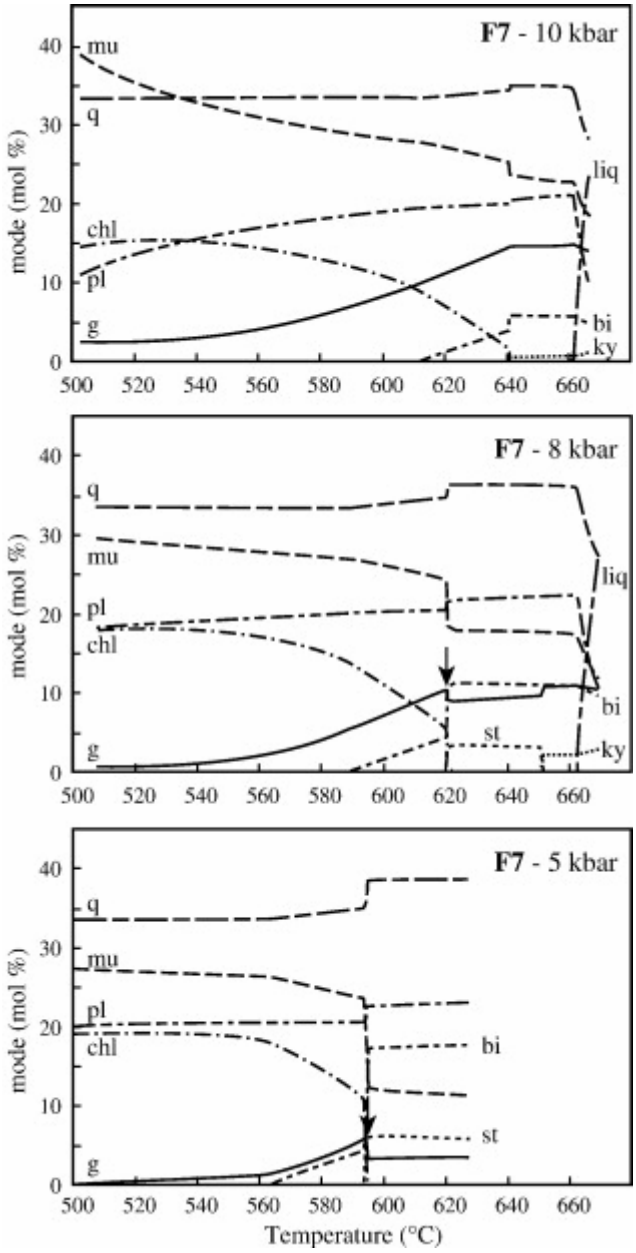

Fig. 11. Modal compositions of sample F7 calculated with THERMOCALC 3.21 at 10 kbar, 8 kbar and 5 kbar, assuming that the system is just at water saturation. Arrows indicate the temperatures at which a garnet resorption takes place in the subsolidus domain due to staurolite nucleation and growth.

Tables

Table 1. : Mineral assemblages of six metapelites of the TPU in the Quercy area (Leyme Unit)

Sample	**F4**	**F6**	**F7**	**F13**	**F24**	**F29**
Main paragenesis						
q	+	+	+	+	+	+
pl	+	+	+	+	+	+
mu	+	+	+	+	+	+
bi	+	+	+	+	+	+
g	+	+	+	+	+	+
st					+	
rt	+	+	+	+	+	+
ap	+	+	+	+	+	
mo	+	+	+	+	+	+
Inclusions in garnet						
q	+	+	+	+	+	+
pl	+	+	+	+	+	+
mu						
bi						
ilm	+	+	+	+	+	+
ap	+	+	+	+	+	+
xe				+		
mo	+	+	+	+	+	+
gr	+					
Secondary minerals						
chl				+		

Table 2. : Bulk chemical compositions of six garnet metapelites of the TPU in the Quercy area (Leyme Unit)

Sample	**F4**	**F6**	**F7**	**F13**	**F24**	**F29**
Weight percent oxides						
SiO_2	58.07	63.03	64.90	76.81	56.90	62.45
Al_2O_3	18.27	18.49	16.80	9.64	19.06	17.79
TiO_2	0.94	0.97	0.80	0.58	0.98	0.82
$(Fe_2O_3)_{tot}$	8.07	7.07	6.52	6.67	7.82	6.98
MgO	3.09	2.73	2.10	1.36	2.96	2.39
MnO	0.13	0.17	0.10	0.07	0.10	0.08
CaO	1.99	0.89	0.73	0.59	1.07	0.47
Na_2O	4.52	2.41	2.46	1.31	2.51	1.34
K_2O	2.04	3.10	2.85	1.97	3.46	4.01
P_2O_5	0.15	0.13	0.07	0.06	0.12	0.06
Total	*97.27*	*98.99*	*97.33*	*99.06*	*94.98*	*96.39*
Mole percent oxides in the model system MnNCKFMAS						
SiO_2	66.41	71.04	73.83	82.81	67.50	72.47
Al_2O_3	12.31	12.28	11.26	6.12	13.32	12.17
FeO_{tot}	6.95	6.00	5.58	5.41	6.98	6.10
MgO	5.27	4.59	3.56	2.19	5.23	4.13
MnO	0.13	0.16	0.10	0.06	0.10	0.08
CaO	2.44	1.07	0.89	0.68	1.36	0.58
Na_2O	5.01	2.63	2.71	1.37	2.89	1.51
K_2O	1.49	2.23	2.07	1.35	2.62	2.97
Mole percent oxides in the model system MnNCKFMA						
Al_2O_3	36.66	42.40	43.03	35.63	40.99	44.18
FeO_{tot}	20.68	20.70	21.33	31.48	21.48	22.14
MgO	15.68	15.84	13.61	12.71	16.10	15.01

Sample	F4	F6	F7	F13	F24	F29
MnO	0.37	0.56	0.37	0.37	0.31	0.29
CaO	7.26	3.71	3.40	3.96	4.18	2.12
Na_2O	14.92	9.09	10.37	7.96	8.88	5.48
K_2O	4.43	7.69	7.90	7.88	8.05	10.78
Parameters calculated from mole percent oxides						
A'[a]	0.03	0.15	0.14	0.00	0.09	0.10
FeO/(FeO + MgO)	0.57	0.57	0.61	0.71	0.57	0.60
CaO/(CaO + Na_2O)	0.33	0.29	0.25	0.33	0.32	0.28

[a] $(Al_2O_3–3K_2O–CaO–Na_2O)/(Al_2O_3–3K_2O–CaO–Na_2O + FeO + MgO)$.

Table 3. : Representative garnet analyses from six metapelites of the TPU in the Quercy area (Leyme Unit)

Sample	**F4**	**F4**	**F6**	**F6**	**F7**	**F7**	**F13**	**F13**	**F24**	**F24**	**F29**	**F29**
Location	**Core**	**Rim**	**Core**	**Rim**	**Core**	**Rim**	**Core**	**Rim**	**Core**	**Rim**	**Core**	**Rim**
Electron microprobe analyses in wt. %												
SiO_2	38.69	38.57	38.66	37.93	37.01	38.35	37.13	37.21	37.68	38.54	36.95	36.83
Al_2O_3	21.15	21.93	21.30	21.61	20.75	21.48	21.37	21.35	21.40	22.17	20.88	21.12
TiO_2	0.13	0.00	0.10	0.07	0.14	0.03	0.05	0.03	0.15	0.06	0.16	0.00
Cr_2O_3	0.00	0.00	0.00	0.00	0.04	0.03	0.04	0.02	0.03	0.00	0.11	0.00
MgO	0.70	2.56	1.76	2.37	0.76	2.71	1.53	2.20	2.29	2.79	0.97	3.40
FeO	20.32	32.83	28.10	31.58	23.05	33.38	32.29	36.71	29.28	34.19	24.82	33.75
MnO	12.15	4.18	10.61	5.74	8.73	1.70	6.54	1.14	8.34	3.28	7.27	1.96
CaO	7.95	1.74	1.84	1.61	9.16	2.93	2.28	1.13	2.44	2.01	7.83	1.76
Total	*101.09*	*101.81*	*102.37*	*100.91*	*99.64*	*100.61*	*101.23*	*99.79*	*101.61*	*103.04*	*98.99*	*98.82*
Structural formulae on a basis of 8 cations and 12 oxygens												
Si^{IV}	3.078	3.052	3.065	3.035	2.984	3.060	2.981	3.020	2.996	3.011	3.001	2.989
Al^{VI}	1.983	2.045	1.990	2.038	1.972	2.020	2.022	2.042	2.005	2.041	1.998	2.010
Ti^{VI}	0.008	0.000	0.006	0.004	0.008	0.002	0.003	0.002	0.009	0.004	0.010	0.000
Cr^{VI}	0.000	0.000	0.000	0.000	0.003	0.002	0.003	0.001	0.002	0.000	0.007	0.000
$(Fe^{3+})^{VI}$	0.000	0.000	0.000	0.000	0.041	0.000	0.008	0.000	0.000	0.000	0.000	0.001
$(Fe^{2+})^{VIII}$	0.083	0.302	1.863	2.113	1.514	2.228	2.160	2.492	1.947	2.234	1.686	2.290

Sample	**F4**	**F4**	**F6**	**F6**	**F7**	**F7**	**F13**	**F13**	**F24**	**F24**	**F29**	**F29**
Location	**Core**	**Rim**	**Core**	**Rim**	**Core**	**Rim**	**Core**	**Rim**	**Core**	**Rim**	**Core**	**Rim**
Mg^{VIII}	1.352	2.173	0.208	0.283	0.091	0.322	0.183	0.266	0.271	0.325	0.117	0.411
Mn^{VIII}	0.819	0.280	0.712	0.389	0.596	0.115	0.445	0.078	0.562	0.217	0.500	0.135
Ca^{VIII}	0.678	0.148	0.156	0.138	0.791	0.251	0.196	0.098	0.208	0.168	0.681	0.153
Mole fractions												
$X_{Fe}^{g} = Fe^{2+}/(Fe^{2+} + Mg)$	0.94	0.88	0.90	0.88	0.94	0.87	0.92	0.90	0.88	0.87	0.93	0.85
$X_{Ca}^{g} = Ca/(Fe^{2+} + Mg + Mn + Ca)$	0.23	0.05	0.05	0.05	0.26	0.09	0.07	0.03	0.07	0.06	0.23	0.05
$X_{Mn}^{g} = Mn/(Fe^{2+} + Mg + Mn + Ca)$	0.28	0.10	0.24	0.13	0.20	0.04	0.15	0.03	0.19	0.07	0.17	0.05
Almandine	0.46	0.75	0.63	0.72	0.51	0.76	0.72	0.85	0.65	0.76	0.56	0.77
Pyrope	0.03	0.10	0.07	0.10	0.03	0.11	0.06	0.09	0.09	0.11	0.04	0.14

Table 4. : Representative biotite analyses from six metapelites of the TPU in the Quercy area (Leyme Unit)

sample	**F4**	**F4**	**F6**	**F6**	**F7**	**F7**	**F13**	**F13**	**F24**	**F24**	**F29**	**F29**
Electron microprobe analyses in wt. %												
SiO_2	36.49	35.58	*34.58*	36.79	36.01	35.71	35.63	36.01	36.79	37.26	36.97	36.17
Al_2O_3	19.64	19.99	*19.79*	19.91	20.21	20.68	19.42	19.64	20.37	20.53	20.21	19.88
TiO_2	1.39	1.15	*1.63*	1.77	2.00	1.68	1.68	1.72	1.93	1.48	1.81	2.18
FeO_{tot}	17.97	18.04	*20.63*	19.67	17.90	17.82	24.60	24.52	17.97	17.27	19.00	19.92
MgO	10.53	10.68	*9.62*	9.57	9.39	9.41	6.90	6.86	10.75	10.53	9.62	9.62
MnO	0.09	0.11	*0.03*	0.08	0.11	0.00	0.09	0.00	0.05	0.00	0.02	0.11
Na_2O	0.24	0.15	*0.14*	0.23	0.16	0.10	0.29	0.22	0.25	0.16	0.26	0.24
K_2O	8.66	8.19	*7.70*	9.34	7.08	6.87	9.15	9.24	8.10	6.76	8.37	8.84
total	*95.01*	*93.89*	*94.12*	*97.36*	*92.86*	*92.27*	*97.76*	*98.21*	*96.21*	*93.99*	*96.26*	*96.96*
Structural formulae on a basis of 11 oxygens without ferric iron												
Si^{IV}	2.743	2.705	2.655	2.727	2.742	2.729	2.700	2.710	2.716	2.776	2.744	2.693
Al^{IV}	1.257	1.295	1.345	1.273	1.258	1.271	1.300	1.290	1.284	1.224	1.256	1.307
Ti^{VI}	0.079	0.066	0.094	0.099	0.115	0.097	0.096	0.097	0.107	0.083	0.101	0.122
Al^{VI}	0.483	0.496	0.446	0.466	0.555	0.592	0.434	0.452	0.489	0.579	0.511	0.438
Fe^{VI}	1.130	1.147	1.325	1.219	1.140	1.139	1.559	1.543	1.109	1.076	1.179	1.240
Mg^{VI}	1.180	1.210	1.101	1.057	1.066	1.072	0.779	0.769	1.183	1.169	1.064	1.068
Mn^{VI}	0.006	0.007	0.002	0.005	0.007	0.000	0.006	0.000	0.003	0.000	0.001	0.007
Na^{A}	0.035	0.022	*0.021*	0.033	*0.024*	0.015	0.043	0.032	0.036	0.023	0.037	0.035
K^{A}	0.830	0.794	*0.754*	0.883	*0.688*	0.670	0.884	0.887	0.763	0.642	0.792	0.840
Mole fraction												
Fe/(Fe + Mg)	0.49	0.49	0.55	0.54	0.52	0.52	0.67	0.67	0.48	0.48	0.53	0.54

Table 5. : Representative muscovite analyses from six metapelites of the TPU in the Quercy area (Leyme Unit)

Sample	**F4**	**F6**	**F7**	**F7**	**F13**	**F13**	**F24**	**F24**	**F29**	**F29**
Electron microprobe analyses in wt. %										
SiO_2	46.38	46.86	46.37	45.17	46.00	45.70	46.69	45.16	46.68	46.74
Al_2O_3	36.23	37.00	36.97	36.11	36.43	35.35	37.60	36.04	35.82	36.09
TiO_2	0.29	0.21	0.31	0.44	0.26	0.67	0.45	0.39	0.65	0.82
FeO_{tot}	0.40	0.74	1.10	2.45	2.04	1.37	0.86	1.88	0.90	1.00
MgO	0.56	0.42	0.49	0.54	0.35	0.44	0.58	0.53	0.63	0.59
MnO	0.14	0.02	0.05	0.06	0.00	0.01	0.13	0.00	0.00	0.00
Na_2O	0.97	1.47	1.08	0.96	1.10	1.34	1.52	0.96	1.07	1.14
K_2O	9.28	8.06	8.09	8.03	8.92	9.27	8.20	8.66	9.53	9.31
Total	*94.25*	*94.78*	*94.47*	*93.76*	*95.10*	*94.15*	*96.03*	*93.65*	*95.28*	*95.69*
Structural formulae on a basis of 11 oxygens without ferric iron										
Si^T	3.085	3.082	3.064	3.033	3.052	3.067	3.040	3.039	3.085	3.074
Ti^T	0.015	0.010	0.015	0.022	0.013	0.034	0.022	0.020	0.032	0.041
Al^T	0.901	0.908	0.921	0.944	0.935	0.900	0.938	0.941	0.883	0.886
Al^{M2}	1.939	1.960	1.958	1.914	1.914	1.896	1.948	1.917	1.906	1.911
Mg^{M2}	0.044	0.020	0.018	0.024	0.020	0.038	0.028	0.028	0.052	0.045
Fe^{M2}	0.017	0.020	0.023	0.062	0.066	0.066	0.024	0.055	0.042	0.043
Mg^{M1}	0.012	0.021	0.030	0.030	0.015	0.006	0.028	0.025	0.010	0.012
Fe^{M1}	0.005	0.021	0.038	0.076	0.047	0.011	0.023	0.050	0.008	0.012
v^{M1}	0.983	0.959	0.933	0.895	0.938	0.983	0.949	0.924	0.982	0.976
Na^A	0.125	0.187	0.138	0.125	0.142	0.174	0.192	0.125	0.137	0.145
K^A	0.787	0.676	0.682	0.688	0.755	0.794	0.681	0.743	0.803	0.781
v^A	0.088	0.136	0.180	0.187	0.103	0.032	0.127	0.131	0.060	0.074
Mole fractions										
Fe/(Fe + Mg)	0.29	0.50	0.56	0.72	0.77	0.64	0.45	0.67	0.44	0.49
Na/(Na + K)	0.14	0.22	0.17	0.15	0.16	0.18	0.22	0.14	0.15	0.16

Sample	**F4**	**F6**	**F7**	**F7**	**F13**	**F13**	**F24**	**F24**	**F29**	**F29**
Paragonite	0.14	0.22	0.17	0.15	0.16	0.18	0.22	0.14	0.15	0.16
Celadonite	0.06	0.04	0.04	0.08	0.09	0.11	0.05	0.09	0.09	0.09
Muscovite	0.80	0.74	0.79	0.76	0.76	0.72	0.73	0.77	0.76	0.75

Table 6. : Representative plagioclase analyses from six metapelites of the TPU in the Quercy area (Leyme Unit)

Sample	**F4**	**F4**	**F6**	**F6**	**F7**	**F7**	**F13**	**F13**	**F24**	**F24**	**F29**
	Matrix	**Matrix**	**Matrix**	**Garnet incl.**	**Matrix**	**Matrix**	**Matrix core**	**Matrix rim**	**Matrix**	**Matrix**	**Matrix**
Electron microprobe analyses in wt. %											
SiO_2	60.68	60.75	62.35	63.32	61.97	61.49	63.28	63.29	60.25	61.14	61.16
Al_2O_3	22.98	22.80	22.45	23.71	23.21	22.96	23.06	22.57	24.46	24.34	22.80
CaO	4.59	4.75	3.59	4.83	4.13	4.03	4.49	3.64	5.69	5.40	3.99
Na_2O	8.86	8.81	8.52	8.74	9.35	9.37	9.00	9.54	8.76	8.75	9.30
K_2O	0.07	0.06	0.70	0.07	0.09	0.24	0.07	0.08	0.05	0.06	0.11
Total	*97.18*	*97.17*	*97.61*	*100.67*	*98.76*	*98.09*	*99.90*	*99.11*	*99.20*	*99.68*	*97.36*
Structural formulae on a basis of 8 oxygens											
Si^{IV}	2.77	2.77	2.82	2.78	2.78	2.78	2.80	2.82	2.70	2.72	2.78
Al^{IV}	1.23	1.22	1.20	1.23	1.23	1.22	1.20	1.18	1.29	1.28	1.22
$Total^{IV}$	*4.00*	*3.99*	*4.02*	*4.01*	*4.00*	*4.00*	*4.00*	*4.00*	*4.00*	*4.00*	*4.00*
Ca^{M}	0.22	0.23	0.17	0.23	0.20	0.20	0.21	0.17	0.27	0.26	0.19
Na^{M}	0.78	0.78	0.75	0.74	0.81	0.82	0.77	0.82	0.76	0.76	0.82
K^{M}	0.00	0.00	0.04	0.00	0.01	0.01	0.00	0.00	0.00	0.00	0.01
$Total^{M}$	*1.01*	*1.01*	*0.96*	*0.98*	*1.02*	*1.03*	*0.99*	*1.00*	*1.04*	*1.02*	*1.02*
Mole fractions											
Albite	0.77	0.77	0.78	0.76	0.80	0.80	0.78	0.82	0.73	0.74	0.80
Anorthite	0.22	0.23	0.18	0.23	0.19	0.19	0.22	0.17	0.26	0.25	0.19

Sample	**F4**	**F4**	**F6**	**F6**	**F7**	**F7**	**F13**	**F13**	**F24**	**F24**	**F29**
	Matrix	**Matrix**	**Matrix**	**Garnet incl.**	**Matrix**	**Matrix**	**Matrix core**	**Matrix rim**	**Matrix**	**Matrix**	**Matrix**
K feldspar	0.00	0.00	0.04	0.00	0.01	0.01	0.00	0.01	0.00	0.00	0.01

Table 7. : Representative staurolite analyses from one metapelite of the TPU in the Quercy area (Leyme Unit)

Sample	**F24**	**F24**	**F24**
Electron microprobe analyses in wt. %			
SiO_2	28.37	28.32	28.54
Al_2O_3	53.35	53.30	53.77
TiO_2	0.51	0.41	0.39
FeO_{tot}	13.47	14.15	13.90
MgO	1.67	1.74	1.73
MnO	0.23	0.12	0.22
ZnO	0.36	0.23	0.20
Total	*97.97*	*98.27*	*98.74*
Formulae on a basis of 46 oxygens without ferric iron			
Si	7.86	7.84	7.85
Ti	0.11	0.08	0.08
Al	17.42	17.39	17.43
Fe	3.12	3.28	3.20
Mg	0.69	0.72	0.71
Mn	0.05	0.03	0.05
Zn	0.07	0.05	0.04
Mole fraction			
Fe/(Fe + Mg)	0.82	0.82	0.82
Zn/(Fe + Mg + Mn + Zn)	0.02	0.01	0.01

Table 8. : *P–T* conditions of metamorphic peaks for six metapelites of the TPU in the Quercy area (Leyme Unit)

Sample	Independent set of reactions	Results
F4	1) mu + 2phl + 6q = py + 3cel	*P* = 7.9 +/− 1.2 kbar
	2) cel + east = mu + phl	*T* = 617 +/− 32 °C
	3) phl + 3an = py + gr + mu	*cor = 0.774*
	4) ann + 3 an = gr + alm + mu	*sigfit = 0.81 (1.61)*
	5) py + 2pa + 3cel = 3 east + 2ab + 9q + $2H_2O$	
F6	1) 3east + 6q = py + phl + 2mu	*P* = 6.6 +/− 1.2 kbar
	2) phl + east + 6q = py + 2cel	*T* = 617 +/− 33 °C
	3) phl + 3an = py + gr +mu	*cor = 0.754*
	4) ann + 3 an = gr + alm + mu	*sigfit = 0.75 (1.61)*
	5) py + 3ann + 2pa + 9q = 3 alm + 2ab + $2H_2O$	
F7	1) 2east + 6q = py + mu + cel	*P* = 9.0 +/− 1.3 kbar
	2) 3east + 6q = py + phl + 2mu	*T* = 655 +/− 34 °C
	3) phl + 3an = py + gr + mu	*cor = 0.763*
	4) ann + 3 an = gr + alm + mu	*sigfit = 0.79 (1.61)*
	5) py + 2pa + 3cel = 3 east + 2ab + 9q + $2H_2O$	
F13	1) mu + 2phl + 6q = py + 3cel	*P* = 5.8 +/− 1.2 kbar
	2) 2east + 6q = py + mu + cel	*T* = 615 +/− 30 °C
	3) phl + 3an = py + gr + mu	*cor = 0.732*
	4) ann + 3 an = gr + alm + mu	*sigfit = 0.20 (1.61)*
	5) py + 2pa + 3cel = 3 east + 2ab + 9q + $2H_2O$	
F24	1) mu + 2phl + 6q = py + 3cel	*P* = 6.7 +/− 1.2 kbar
	2) 2east + 6q = py + mu + cel	*T* = 644 +/− 32 °C
	3) 5 py + 23cel + 2mst = 23 east + 76 q + $4H_2O$	*cor = 0.845*
	4) 23ann + 6fst + 48q = 31alm + 23mu + $12H_2O$	*sigfit = 0.76 (1.49)*
	5) phl + 3an = py + gr + mu	
	6) 17east + 4ab + 2mst + 44q = 14py + 17mu + 4pa	

Sample	Independent set of reactions	Results
	7) 17ann + 12ab + 6fst + 30q = 25alm + 17mu + 12pa	
F29	1) mu + 2phl + 6q = py + 3cel	*P* = 7.9 +/− 1.2 kbar
	2) cel + east = mu + phl	*T* = 641 +/− 32 °C
	3) phl + 3an = py + gr + mu	*cor = 0.745*
	4) ann + 3 an = gr + alm + mu	*sigfit = 0.29 (1.61)*
	5) py + 2pa + 3cel = 3 east + 2ab + 9q + $2H_2O$	